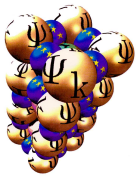

Ψ_k Scientific Highlight Of The Month

No. 121 **February 2014**

Generalized Langevin equation thermostats for *ab initio* molecular dynamics.

Michele Ceriotti[1]

Laboratory of Computational Science and Modelling, Institute of Materials, École Polytechnique Fédérale de Lausanne (EPFL), CH-1015 Lausanne, Switzerland

Abstract

Molecular dynamics can be used as a very effective, general-purpose approach to generate atomic configurations for a material or chemical compound that are consistent with prescribed experimental conditions. It is an ideal companion to *ab initio* electronic structure methods, that allow one to evaluate the inter-atomic forces from first principles, avoiding the time-consuming and at times inaccurate process of designing an empirical model. Unfortunately, *ab initio* methods are still computationally demanding, and so it is desirable to modify the properties of the dynamics to get a more effective exploration of phase space than allowed by the intrinsic system's dynamics. A very effective approach to manipulate the sampling behaviour of a molecular dynamics simulation exploits non-Markovian, Generalized Langevin Equations (GLEs) that have been used in the past to model the coupling of the system with a physical bath. Within this framework, the impact of the correlated noise on static and dynamic properties of the trajectory can be predicted analytically in the harmonic limit. One can therefore optimize the performances of the GLE *a priori*, and obtain effects that range from effective sampling of all the relevant time scales, to fine-tuned control of the disturbance of dynamics for different frequency ranges, to the design of non-equilibrium trajectories that can be used to model zero-point energy and other nuclear quantum effects and even to evaluate matrix functions with linear scaling effort. Correlated noise can also be combined with imaginary time path integral molecular dynamics, to obtain fast and systematic convergence of properties that depend on the quantum nature of light nuclei – that are paramount for materials that contain hydrogen. This review will introduce the theoretical basis of the GLE thermostat framework and will briefly discuss the many ways it can be used to manipulate the sampling properties of molecular dynamics. The practical implementation will also be covered, and a few selected applications in the context of *ab initio* molecular dynamics will be presented as examples.

Simulating on a computer the behaviour of matter at the atomic scale can be invaluable in assisting the interpretation of experiments, predicting the properties of materials and determining the reactivity of chemical compounds. The accuracy and predictive power of computational

[1] michele.ceriotti@epfl.ch

modeling is growing constantly, partly because of the exponential increase in hardware performance, and partly because of methodological advances in simulation techniques. In particular, *ab initio* simulations that explicitly take into account the quantum nature of electrons have the advantage that they do not require previous knowledge of the system's properties. Extensions to density functional theory (DFT) [1] to treat more accurately electronic correlations [2] and dispersion forces [3–5] are opening up the possibility of studying materials that exhibit at the same time subtle electronic properties, complex structural features and rich long-time dynamics.

In simple systems, such as crystals and isolated molecules, it is often sufficient to determine the properties of a few selected configurations, corresponding to the minima of the potential energy. For more complex problems such as liquids, or whenever thermal fluctuations are expected to play an important role, an effective simulation will have to generate thousands of configurations so as to compute average values consistent with the reference experimental conditions.

Molecular dynamics (MD) proceeds by integrating Hamilton's equations for the atoms, and is particularly effective in generating sequences of configurations to compute ensemble averages, and under appropriate condition also dynamical properties. Contrary to Monte Carlo sampling, that can be made very efficient but requires deep insight into the problem at hand [6], MD generally yields good sampling performances even when straightforwardly applied to to an unknown system – which makes it an ideal complement to the first-principles evaluation of the electronic structure [7].

The generality of the MD approach does not imply that it is not possible to better its performances by modifying Hamilton's equations. Whenever one is interested in computing properties in constant-temperature conditions, it is possible to introduce so-called thermostats, that introduce fluctuations in the total energy consistent with canonical Boltzmann sampling. In the last few years, a remarkably flexible framework based on a non-Markovian Generalized Langevin Equation (GLE) has been developed [8, 9], that makes it possible to achieve an exquisite control over the sampling properties of a molecular dynamics trajectory, to enhance its sampling efficiency [10–12] and even to model inexpensively the quantum nature of light nuclei [13], also in conjunction with path integral methods [14, 15].

Here, we will review the theoretical foundations of the GLE thermostat framework, and its application to efficient constant-temperature MD and to the modelling of nuclear quantum effects. Particular attention will be paid to the implications of these techniques in the context of *ab initio* electronic structure calculations.

1 Constant-temperature molecular dynamics

Let us consider for a start the case of a particle of mass m described by position q and momentum p, subject to a one-dimensional potential V. Molecular dynamics amounts at integrating Hamilton's equations

$$\begin{aligned} \dot{q} =& p/m \\ \dot{p} =& - V'(q), \end{aligned} \tag{1}$$

to generate a trajectory $(p(t), q(t))$, out of which one wants to extract physical quantities, such as the constant-temperature expectation values of an observable $O(p, q)$.

A trajectory is said to be ergodic for canonical sampling if, in the limit of an infinitely long trajectory, the time average of the observable along the trajectory is equivalent to the average over the Boltzmann distribution at an inverse temperature $\beta = 1/k_B T$:

$$\langle O \rangle = \int O(p,q) e^{-\beta\left[\frac{p^2}{2m}+V(q)\right]} \mathrm{d}p\mathrm{d}q \equiv \lim_{t_{\mathrm{tot}}\to\infty} \frac{1}{t_{\mathrm{tot}}} \int_0^{t_{\mathrm{tot}}} O\left(p(t), q(t)\right) \mathrm{d}t. \tag{2}$$

In practice, the length of a simulation will be limited by computational cost considerations, and it is therefore important that the statistical error inherent in a finite trajectory is as small as possible, particularly in the computationally-demanding case of *ab initio* modelling.

The statistical efficiency of an MD strategy to compute the observable O can be assessed by computing the autocorrelation time of the observable [6, 16]

$$\tau_O = \int_0^{\infty} \langle O(t)O(0) \rangle \, \mathrm{d}t, \tag{3}$$

which is nothing but the integral of the autocorrelation function

$$\langle O(t)O(0) \rangle = \lim_{t_{\mathrm{tot}}\to\infty} \frac{1}{t_{\mathrm{tot}} - t} \int_0^{t_{\mathrm{tot}}-t} \frac{\left(O(p(t+s), q(t+s)) - \langle O \rangle\right)\left(O(p(t), q(t)) - \langle O \rangle\right)}{\sigma^2(O)} \mathrm{d}s, \tag{4}$$

where we introduced the mean and variance of O, $\langle O \rangle$ and $\sigma^2(O)$. In fact, the statistical error in a trajectory of length t_{tot} is $\epsilon^2 \approx \sigma^2(O)\tau_O / t_{\mathrm{tot}}$.

Note that in practice it is much harder to converge the autocorrelation function (4) than it is to converge the expectation value of O, and that in general it is almost impossible to obtain an accurate estimate of the autocorrelation time from a first-principles simulation. Whenever possible, one should perform preliminary simulations using empirical forcefields to estimate the order of magnitude of τ_O, so that the feasibility of an *ab initio* treatment of the problem can be established, and a conservative estimate of the statistical error can be determined.

It is easy to see that Eqs.(1) alone are not sufficient to perform constant-temperature sampling. Hamiltonian dynamics conserves the total energy, and it will be necessary to modify the equations of motion to allow for energy fluctuations. Over the years, many strategies have been designed to this aim, starting from the simple and elegant Andersen thermostat [17], to velocity rescaling and Berendsen thermostat [18] (which do *not* guarantee canonical sampling and should be avoided), to deterministic thermostat of the Nosé-Hoover kind [19–21], and stochastic thermostat based on Langevin dynamics [22–24], which are the basis of the approach discussed here.

1.1 Langevin dynamics

Langevin dynamics was originally introduced as a model for Brownian motion [25], and in its original form describes the motion of the position q of a free particle subject to viscous drag from the surrounding medium $-\gamma\dot{q}$, and to a stochastic force ξ that arises because of the collisions with surrounding molecules:

$$\ddot{q} + \gamma\dot{q} - \xi = 0. \tag{5}$$

Figure 1: Sample trajectory of potential (blue), kinetic(red) and total (black) energy (upper panels) and position (lower panels) for a one-dimensional harmonic oscillator of frequency $\omega = 1$ and mass $m = 1$, at temperature $k_B T = 1$, subject to Langevin dynamics with friction γ. Panel (a): $\gamma = 0$; panel (b): $\gamma = 1$; panel (c): $\gamma = 10^3$. Not that in the over-damped case (c) the diffusion in configuration space is greatly slowed down.

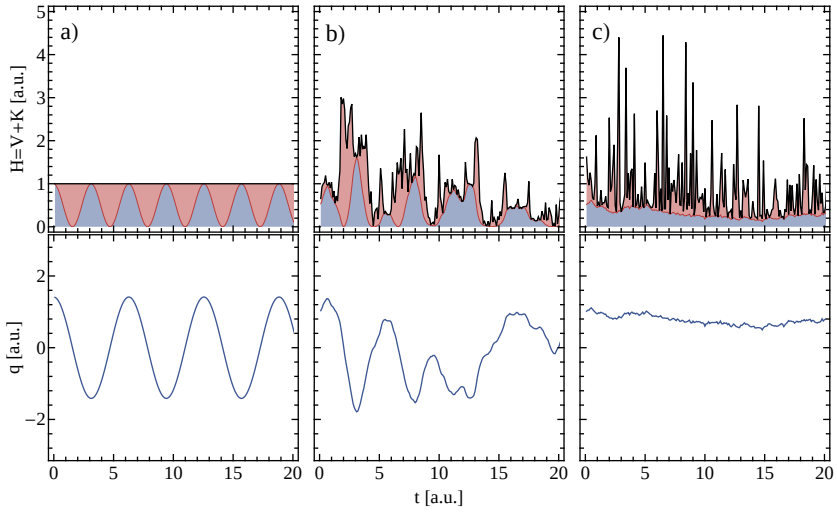

In this simplified model, it is assumed that the interactions between the Brownian particle and its surroundings are instantaneous, which implies that the friction term only depends on the instantaneous value of the velocity, and that the noisy force term (which is a Gaussian variate) has no correlation in time, i.e. $\langle \xi(t)\xi(0) \rangle = \delta(t)$. The model can be also seen as describing the interaction of a system with an infinite thermal bath, and in this sense it has been used for a long time [22] to modify Hamilton's equations to sample the constant-temperature ensemble:

$$\begin{aligned} \dot{q} =& p/m \\ \dot{p} =& -V'(q) - \gamma p + \sqrt{2m\gamma/\beta}\xi(t). \end{aligned} \tag{6}$$

The friction γ determines the impact of the Langevin terms onto the dynamics of the system, and how quickly the total energy of the system fluctuates. One should not think that a larger value of γ necessarily implies more efficient sampling of the canonical ensemble (see Figure 1). It is instructive to consider the case of a harmonic potential $V(q) = m\omega^2 q^2/2$, for which the Langevin dynamics can be solved analytically [26] so that the correlation times of potential, kinetic and total energies can be computed to obtain [9]

$$\tau_K(\omega) = \frac{1}{2\gamma}, \quad \tau_V(\omega) = \frac{1}{2\gamma} + \frac{\gamma}{2\omega^2}, \quad \tau_H(\omega) = \frac{1}{\gamma} + \frac{\gamma}{4\omega^2} \quad . \tag{7}$$

The correlation time of the kinetic energy decreases monotonically as the friction term is increased, but τ_V and τ_H both have an optimal, "critical damping" value corresponding to minimum correlation times, and the sampling efficiency decreases as γ is increased further into an over-damped regime (Figure 2). This is just a manifestation of the fact that it is easy to sample momenta (that are distributed according to a simple, Gaussian distribution) but it is hard to sample configurations, that in general are distributed following a complex, non-linear potential energy function.

Figure 2: Correlation time of potential (τ_V), kinetic (τ_K) and total (τ_H) energy for the white-noise Langevin dynamics of a harmonic oscillator, as a function of the friction γ and the frequency ω.

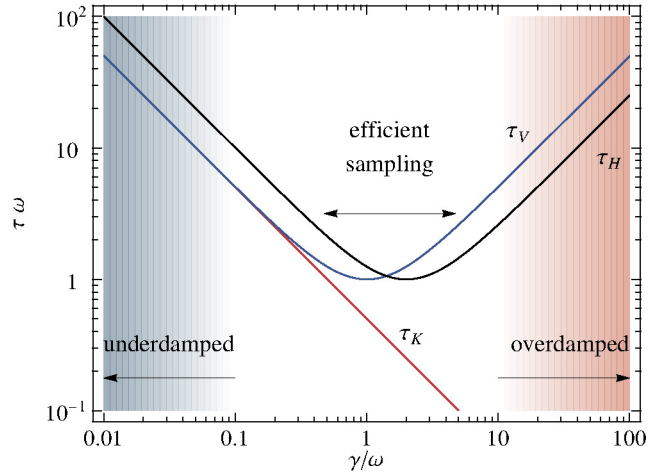

Eqs. (7) imply that for a given vibrational mode there is an optimal friction that yields the best statistical efficiency for the potential energy – that we can consider as a proxy for configurational sampling. In an actual simulation, however, vibrational frequencies will typically span several orders of magnitude, comprising localized, high-frequency modes as well as long wavelength acoustic modes in solids and anharmonic, collective motion in liquids or macromolecules. In these cases, one would need to optimize the choice of friction depending on the property that must be computed, which is clearly inconvenient given that often one wants to evaluate many properties at once and that optimizing sampling efficiency empirically requires time-consuming preparatory simulations. Ideally, one would like to be able to optimize separately the sampling efficiency of each vibrational mode present, so that sampling can proceed as efficiently as possible for any physical property.

Before continuing, let us remark a subtle but important aspect of Langevin dynamics. Consider the Langevin dynamics of a multi-dimensional system, written using mass-scaled variables ($q \leftarrow \sqrt{m}q$, $p \leftarrow p/\sqrt{m}$), so that the dynamics can be expressed in the compact form

$$\begin{aligned} \dot{\mathbf{q}} &= \mathbf{p} \\ \dot{\mathbf{p}} &= -\,\partial V/\partial \mathbf{q} - \gamma \mathbf{p} + \sqrt{2\gamma/\beta}\boldsymbol{\xi}. \end{aligned} \tag{8}$$

Here $\boldsymbol{\xi}$ is a vector of uncorrelated Gaussian random variates, $\langle \xi_i(t)\xi_j(0)\rangle = \delta_{ij}\delta(t)$. Now consider an orthogonal transformation of the coordinates, $\tilde{\mathbf{q}} = \mathbf{O}\mathbf{q}$ and $\tilde{\mathbf{p}} = \mathbf{O}\mathbf{p}$. Because of the orthogonality of $\mathbf{O}$, it is true that $\partial V/\partial\tilde{\mathbf{q}} = \mathbf{O}\partial V/\partial\mathbf{q}$, and that $\left\langle \mathbf{O}\boldsymbol{\xi}(t)\boldsymbol{\xi}(0)^T\mathbf{O}^T\right\rangle = \delta(t)\mathbf{1}$. Thanks to the Gaussian statistics of $\boldsymbol{\xi}$, also the transformed noise $\tilde{\boldsymbol{\xi}} = \mathbf{O}\boldsymbol{\xi}$ has identical Gaussian statistics. Hence, the equations of motion in the transformed coordinates are completely equivalent to those in the original coordinates. The invariance of Langevin dynamics under an orthogonal transformation means for instance that if a Langevin dynamics with friction γ is applied to a multi-dimensional harmonic system, the very same statistical and dynamical properties would be observed if the equations of motion were written in the Cartesian basis or in normal-modes coordinates, i.e. that the predictions of Eqs. (7) apply for each normal mode separately, even

though the dynamics is integrated in Cartesian coordinates without explicit knowledge of the systems's vibrational frequencies or Hessian eigenvectors.

1.2 Generalized Langevin dynamics

The possibility of predicting the sampling behaviour in the harmonic limit – and that the predictions hold irrespective of the basis in which the dynamics is integrated – is a remarkable feature of Langevin dynamics. At the same time, the analysis we performed in the previous section demonstrates why it is difficult to choose an universal value of the friction: each of the vibrational modes in the system would require a different value of γ to be sampled with optimal efficiency. One is then led to consider generalizations of the Langevin equation, that preserve the good features of Eq. (5) while giving more freedom in controlling how Hamiltonian dynamics are modified.

When considering more carefully the effect of the coupling between a physical system and a heat reservoir, a non-Markovian, history-dependent generalized Langevin equation (GLE) arises very naturally [27–32]

$$\begin{aligned} \dot{q} &= p/m \\ \dot{p} &= -V'(q) - \int_{-\infty}^{t} K(t-s)p(s)\mathrm{d}s + \zeta(t), \end{aligned} \tag{9}$$

where $K(t)$ is a friction memory kernel that describes dissipation and $H(t) = \langle \zeta(t)\zeta(0) \rangle$ is the time correlation of the noisy force. Eq. (9) is obtained when the dynamical variables associated with the bath are integrated out, leaving an effective, history-dependent dynamics for the system only. Because of this, GLEs of this form have been used in the past to model an open system coupled to a physical bath [33]. The dynamics described by Eqs. (9) is also promising for our purpose of controlling the sampling and equilibration properties of molecular dynamics [34]. If one considers a multi-dimensional system, with identical non-Markovian dynamics having independent Gaussian ζ applied to the different degrees of freedom, it is easy to see that the same argument discussed above applies, and that the dynamics is invariant to orthogonal transformations of the coordinates. However, the non-Markovian nature of the equations of motion means that it is considerably more complex to derive analytical estimates of the sampling properties in the harmonic limit, and that the practical implementation of the equations of motion would be riddled with difficulties.

To circumvent this inconvenience, we introduced n fictitious degrees of freedom $\mathbf{s}$, and wrote a Markovian Langevin dynamics in an extended phase space [35]

$$\begin{aligned} \dot{q} =& p \\ \begin{pmatrix} \dot{p} \\ \dot{\mathbf{s}} \end{pmatrix} =& \begin{pmatrix} -V'(q) \\ \mathbf{0} \end{pmatrix} - \begin{pmatrix} a_{pp} & \mathbf{a}_p^T \\ \bar{\mathbf{a}}_p & \mathbf{A} \end{pmatrix} \begin{pmatrix} p \\ \mathbf{s} \end{pmatrix} + \begin{pmatrix} b_{pp} & \mathbf{b}_p^T \\ \bar{\mathbf{b}}_p & \mathbf{B} \end{pmatrix} \begin{pmatrix} \\ \boldsymbol{\xi} \\ \\ \end{pmatrix}, \end{aligned} \tag{10}$$

Here, $\boldsymbol{\xi}$ is a vector of $n+1$ uncorrelated Gaussian random numbers, with $\langle \xi_i(t)\, \xi_j(0) \rangle = \delta_{ij}\delta(t)$. Clearly, Eq. (6) is recovered when $n = 0$. It is easy to see, by integrating out the additional degrees of freedom in a Mori-Zwanzig fashion, that Equations (10) are statistically equivalent to Eqs. (9) with $K(t) = 2a_{pp}\delta(t) - \mathbf{a}_p^T e^{-|t|\mathbf{A}} \bar{\mathbf{a}}_p$ and an analogous (albeit more cumbersome)

expression for the noise correlation function $H(t)$ [8, 9]. Note that in order to achieve canonical sampling a fluctuation-dissipation theorem must hold, requiring that the noise and friction memory kernels are related by $H(t) = k_B T K(t)$ [31].

The GLE has hence been reformulated as a linear, Markovian stochastic differential equation, that can be thought as a matrix generalization of conventional, white-noise Langevin dynamics (an Ornstein-Uhlenbeck process [26]). To distinguish expressions where the matrices are restricted to act on $(p, \mathbf{s})$ and expressions where matrices act on the full state vector $\mathbf{x} = (q, p, \mathbf{s})^T$, we will use the same labelling introduced in Refs. [8, 9, 13]:

$$\begin{array}{c|ccc} & q & p & \mathbf{s} \\ q & m_{qq} & m_{qp} & \mathbf{m}_q^T \\ p & \bar{m}_{qp} & m_{pp} & \mathbf{m}_p^T \\ \mathbf{s} & \bar{\mathbf{m}}_q & \bar{\mathbf{m}}_p & \mathbf{M} \end{array} \quad \left.\begin{array}{l} \\ \\ \end{array}\right\}\mathbf{M}_p \quad \left.\begin{array}{l} \\ \\ \\ \end{array}\right\}\mathbf{M}_{qp} \tag{11}$$

The form of Eqs. (10) is very general, and comprises as special cases many related GLE implementations [36, 37], that have on their side a more transparent relation to a physical model of the bath. Here we are only interested in obtaining the maximum flexibility with the most compact formulation possible, and will therefore derive all of our results in the general case of arbitrary $\mathbf{A}_p$ and $\mathbf{B}_p$ matrices. $\mathbf{A}_p$ and $\mathbf{B}_p$ determine the static covariance matrix $\mathbf{C}_p$, that determines the fluctuations of p and $\mathbf{s}$ in the free-particle limit. In fact, the three matrices must satisfy the relation $\mathbf{A}_p\mathbf{C}_p + \mathbf{C}_p\mathbf{A}_p^T = \mathbf{B}_p\mathbf{B}_p^T$. Furthermore, one can show that a sufficient condition to fulfill fluctuation-dissipation theorem and achieve canonical sampling is that $\mathbf{C}_p = k_B T$, so that in practice if one wants to sample configurations consistent with Boltzmann statistics the diffusion matrix $\mathbf{B}_p$ is determined by the value of $\mathbf{A}_p$ via $\mathbf{B}_p\mathbf{B}_p^T = k_B T \left(\mathbf{A}_p + \mathbf{A}_p^T\right)$.

It is easy to see that the dynamics of a multi-dimensional generalization in which equivalent (same-parameters) but independent (uncorrelated) GLEs are applied to individual degrees of freedom of the system are rotationally invariant. Thus, predictions for the statistical and dynamical properties of a one-dimensional harmonic oscillator will be realized on each vibrational mode of a real system, regardless of whether the GLE is integrated in the normal-modes or in the Cartesian basis. Contrary to the explicitly non-Markovian case, it is now possible to solve the harmonic case analytically, since the dynamics for $\mathbf{x} = (q, p, \mathbf{s})^T$ reads simply

$$\dot{\mathbf{x}} = -\mathbf{A}_{qp}\mathbf{x} + \mathbf{B}_{qp}\boldsymbol{\xi}, \text{where } \mathbf{A}_{qp} = \begin{pmatrix} 0 & -1/m & \mathbf{0} \\ \omega^2 & & \\ \mathbf{0} & \mathbf{A}_p & \end{pmatrix} \quad \mathbf{B}_{qp} = \begin{pmatrix} 0 & 0 & \mathbf{0} \\ 0 & & \\ \mathbf{0} & \mathbf{B}_p & \end{pmatrix} \tag{12}$$

which is in itself just an Ornstein-Uhlenbeck process.

Refs. [8, 9] report the expressions for a number of static and dynamic properties of the dynamics of a harmonic oscillator of frequency ω as a function of the parameters $\mathbf{A}_p$ and $\mathbf{B}_p$. These include expressions for the correlation times (7), that are cumbersome but straightforward, basically requiring diagonalisation of small matrices of size $n + 2$. It is therefore possible to evaluate the sampling properties of the GLE exactly, without statistical error and without having to run test calculations. Furthermore, the dynamics of a multi-dimensional harmonic system will comply with these predictions without having to know explicitly the vibrational modes. This makes it possible to design GLE dynamics that address the problem of efficient sampling, that is crucial

in order to obtain converged thermal averages within the limited simulation time accessible by *ab initio* MD.

2 Custom-tailored GLE thermostats

Depending on the number of additional degrees of freedom n, the GLE thermostat involves a large number of parameters, and it would be completely impractical to choose them by trial and error, based on test simulations for a specific system. For this approach to be useful, the parameters have to be decided *a priori*, based on the analytical estimates that can be computed in the harmonic limit.

Let us focus for instance on the task of optimising the sampling efficiency for the potential energy of the harmonic oscillator. For a given frequency ω the minimal correlation time is obtained for $\gamma = \omega$, and equals $1/\omega$ – i.e. slower modes imply longer correlation times even in the best case scenario. It is therefore useful to introduce $\kappa_V = 1/\tau_V\omega$ as a normalized measure of sampling efficiency, which is 1 in the optimal case and smaller for sub-optimal sampling.

The strategy for designing a transferable "optimal sampling" GLE is quickly explained. The only piece of information that is needed is a rough estimate of the range of frequencies that is needed for the problem at hand (e.g. 1 to 4000 cm^{-1} for a liquid containing O–H bonds). Then, one can start from a tentative (e.g. random) $\mathbf{A}_p$ matrix, and compute the value of κ_V for a number of $\omega \in [1, 4000]\mathrm{cm}^{-1}$. The elements of $\mathbf{A}_p$ can then be modified, so as to iteratively optimize the values of κ_V across the chosen frequency range, aiming for a large, constant value of the sampling efficiency.

The details of the fitting procedure have been discussed in Refs. [8, 9], and will not be repeated here. One important aspect is the need of parametrising $\mathbf{A}_p$ (and in some cases $\mathbf{B}_p$) in a way that enforces automatically some mathematical constraints that must be fulfilled in order to get a well-behaved stochastic dynamics (e.g. the eigenvalues of $\mathbf{A}_p$ must have positive-definite real part). An objective function is then introduced that evaluates how much the GLE generated by the tentative set of parameters deviates from the desiderata (e.g. large and constant κ_V). A minimum is then found by iteratively changing the parameters, for instance using Nelder-Mead downhill simplex algorithm [38].

The response of the GLE as a function of frequency is typically very smooth (in fact, it takes considerable effort to obtain fits with sharp changes as a function of ω), so it is not worth to target specifically the vibrational density of states of a given system. Asking for equally efficient sampling of all vibrational modes over a broad range of frequencies yields a very transferable set of parameters, that can be used to obtain efficient sampling for many different systems without the need of time-consuming preliminary tests.

2.1 Smart sampling GLE

If one observes carefully the $\kappa_V(\omega)$ curves optimised over different frequency ranges (Figure 3), it becomes apparent that there is a trade-off between the breadth of the range and the constant sampling efficiency that can be achieved. At the extremes of the fitted range the GLE is orders

Figure 3: Sampling efficiency for the potential energy, κ_V, for different optimal sampling GLE thermostat, that have been designed to yield constant mormalized efficiency over different ranges of frequency (two, four, six orders of magnitude from bottom to top). Red lines are obtained from matrices with $n = 2$, blue lines are the best fit for matrices with $n = 4$, and the black line is the most balanced choice of white noise, shown as reference.

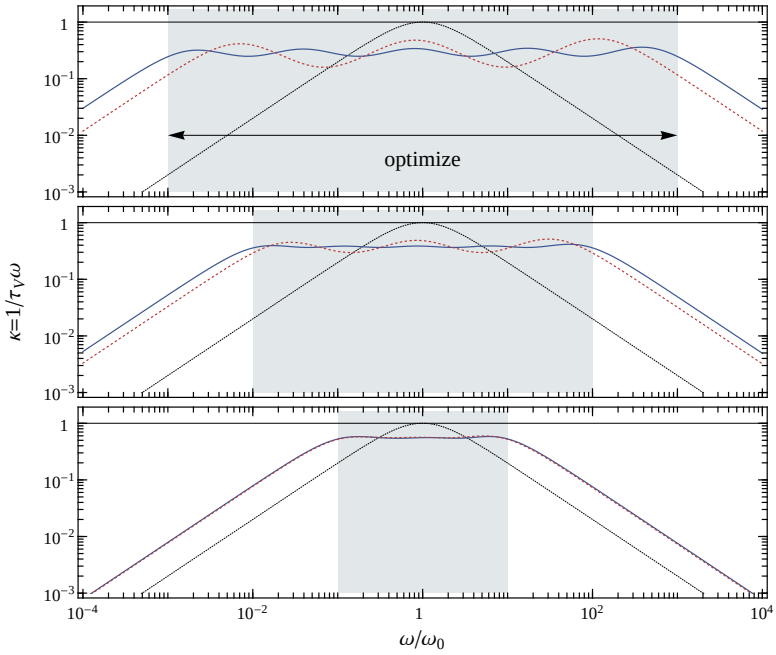

of magnitude more effective than the best choice of white noise, however the GLE constant κ_V is about 50% of the ideal value of 1, and tends to be lower for the broader fitting ranges.

While an "optimal sampling" GLE guarantees that no vibrational mode is severely over or under-damped, one could argue that treating evenly all vibrational modes is not the best choice possible. Slow, collective modes are the most challenging, while fast vibrations will be sampled several times during the simulation, and so achieving optimal sampling efficiency is less crucial. A smarter sampling strategy would be to consider an estimate of the maximum simulation time one can afford $t_{\max}$, and to ensure that vibrations with frequency $\omega_{\min} = 2\pi/t_{\max}$ (the slowest one can hope to observe) are sampled with maximum efficiency. All the faster modes, up to the maximum frequency present $\omega_{\max}$, should be sampled as efficiently as possible, *without negatively affecting the sampling of slower modes*. In practice, we found that it is possible to obtain a decay of $\kappa_V(\omega) \sim 1/\sqrt{\omega}$ above $\omega_{\min}$ – rather than the $1/\omega$ decay that would be expected for white noise (see Figure 4).

As shown in Figure 5, in a practical case (a MD simulation of liquid water at room temperature) this leads to a shorter correlation time for a hard-to-compute property such as the cell dipole moment, and a slightly longer correlation time for the potential energy, that has a short correlation time and is easy to converge anyway. This example demonstrates on one hand that a "smart-sampling" GLE helps ensuring that as much statistics as possible is extracted from demanding MD simulations, and on the other hand illustrates the philosophy of GLE thermostatting: a set of parameters is optimized based on very general considerations and analytical estimates in the harmonic limit, and then it is applied to a real, complex simulation yielding results that are

Figure 4: Sampling efficiency for the potential energy κ_V as a function of the frequency, for a white-noise thermostat optimised for $\omega = 0.4\text{cm}^{-1}$ (black), for a optimal sampling GLE optimised between 0.4 and 4000cm^{-1} (red) and for smart sampling GLE optimised between 0.4 and 4000cm^{-1} (blue). The upper panel shows the velocity-velocity correlation spectrum for a flexible TIP4P water model [39], as reference.

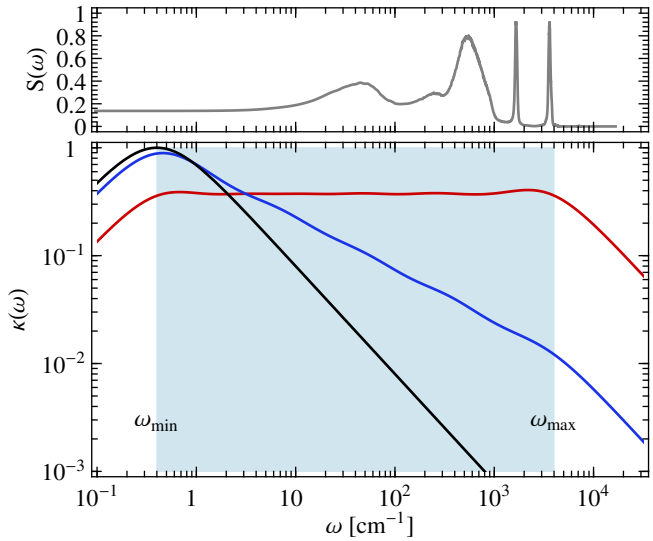

Figure 5: Autocorrelation functions of the potential energy (top) and the components of the total dipole moment of the simulation cell (bottom, $\langle \mathbf{d}(0) \cdot \mathbf{d}(t) \rangle$), for a simulation of a flexible water model [39]. The different curves correspond to simulations performed with a white-noise Langevin thermostat optimised for $\omega = 0.4\text{cm}^{-1}$ (black), for a optimal sampling GLE optimised between 0.4 and 4000 cm^{-1} (red) and for smart sampling GLE optimised between 0.4 and 4000 cm^{-1} (blue). Note that smart-sampling has comparable performance to a very weak Langevin thermostat for hard-to-compute properties depending on slow collective rearrangement of atoms, while being dramatically more efficient for faster-converging properties such as the potential energy.

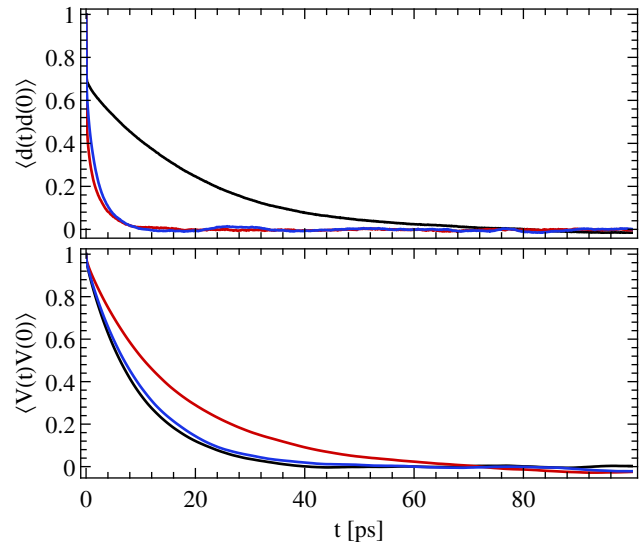

Figure 6: Drift of the kinetic energy associated with the electronic variational parameters in the CPMD dynamics of a water molecule [10]. Panel (a) shows the results with a strongly-damped ($\gamma = 15$fs) Langevin dynamics, panel (b) using a GLE specifically designed to maintain adiabatic decoupling, and panel (c) using massive Nosé-Hoover chains.

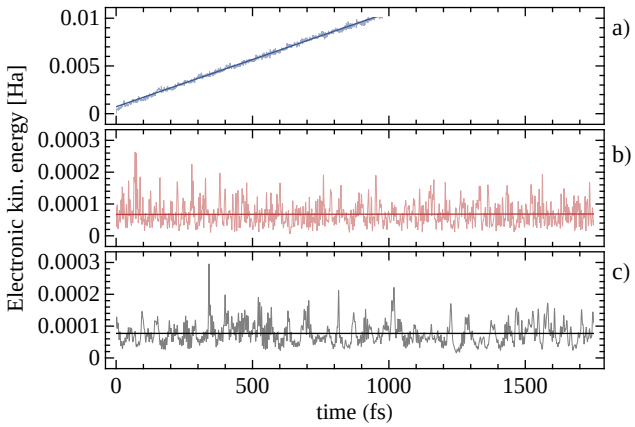

compatible with the initial set of desiderata.

2.2 Maintaining adiabatic decoupling in Car-Parrinello MD

Optimal sampling and – to a lesser extent – smart sampling both introduce a strong noisy force term, that modifies the dynamics of the system and contains high-frequency components. This is not a problem when performing Born-Oppenheimer MD (see below for a discussion of the impact on the conserved quantity and the accuracy of sampling), but it requires some care when performing a combined electron-nuclei dynamics such as Car-Parrinello MD [7], or similar methods based on adiabatic decoupling of some "fast" degrees of freedom relative to the motion of the nuclei[40–44].

The idea behind CPMD-like methods is very general, and can be applied to any simulation that requires variational optimization of a set of parameters for each configuration of the nuclei. A fictitious mass is associated to the parameters that should be optimised, and an artificial dynamics is defined in which the nuclear degrees of freedom and the variational parameters are evolved simultaneously. If the variational parameters are optimised at the beginning of the trajectory, they will evolve staying close to the ground state, provided that their dynamics is kept adiabatically decoupled from that of the nuclei by choosing a suitably small fictitious mass.

White-noise Langevin dynamics has a disruptive effect on CPMD, because the power spectrum of the noisy forces acting on the nuclei contains very high frequencies, and hence interferes with the dynamics of the variational parameters. Their fictitious kinetic energy grows rapidly (see Figure 6) and the nuclear dynamics deviates dramatically from the desired ground-state conditions. Because of this, Nosé-Hoover-style deterministic thermostats [19–21] have generally been used in these kind of simulations, as they do not introduce very high frequency motion in the nuclear dynamics. However, they do not offer the same flexibility as GLE thermostats, require a complex multiple-time step integration, and in the *massive* (one chain per degree of freedom) case have the inelegant property of not being invariant to rigid rotations of the system [9].

Figure 7: (a) Autocorrelation function of the squared symmetric stretching coordinate for the CPMD of a single water molecule in vacuum. The blue curve corresponds to NHC thermostatting, and the red curve to a GLE thermostat designed to sample efficiently ionic degrees of freedom without affecting high-frequency modes. (b) Autocorrelation function of the squared bending coordinate. The inset shows the sampling efficiency κ_H for the GLE dynamics used for sampling. Curves use the same color code as in panel (a).

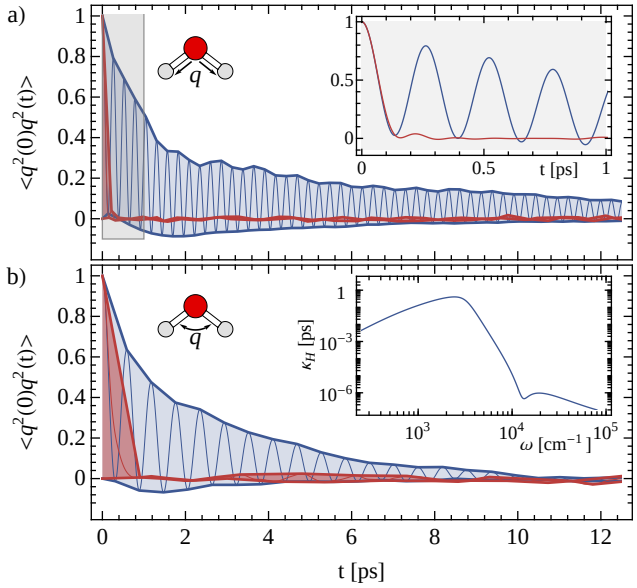

Luckily, generalized Langevin dynamics is flexible enough to be modified so that it does not disturb adiabatic decoupling. In fact, the first application of GLE thermostats was precisely aimed at introducing a low-pass filter on the noise, to make stochastic dynamics compatible with CPMD [10]. Figure 6b shows that filtered Langevin dynamics does indeed maintain adiabatic decoupling, while Fig. 7 demonstrates that, by an a-priori tuning of the sampling efficiency over the ionic frequency range, it is possible to significantly improve equilibration and sampling relative to NHC thermostatting [10].

2.3 Stabilizing multiple time-step dynamics

As a final demonstration of the flexibility of GLE thermostats, let us consider the problem of stabilising multiple time step dynamics. Whenever it is possible to decompose the inter-atomic forces in a fast (and inexpensive) component and one slowly-varying (and expensive) one, it is possible and advantageous to introduce a multiple time step procedure [45, 46], whereby the fast component of the force is evaluated often, and the slow component is evaluated once every several steps, reducing dramatically the cost of the simulation while maintaining an accurate description of the physics. These methods are common when using empirical force fields, where the slowly-varying component of the force typically corresponds to long-range electrostatics. More recently, attempts have been made to develop similar schemes for ab initio MD [47, 48], although the partitioning of the forces in slow and fast components is less obvious.

In either case, it is known that even with an effective splitting there is a limit to the ratio between the slower and the faster time steps, because the fast degrees of freedom in the system

enter in resonance with the small errors in the seldom-updated slow component [49]. It is also well-known that such "resonance barrier" can be overcome by coupling the system to a strong thermostatting bath [50]. However, as we have seen above, over-damped thermostatting reduces the sampling efficiency of diffusive modes, so that despite the larger outer time step, little or no advantage is obtained in terms of statistical efficiency.

Ideally, one would like to use a thermostat that is active on the fast degrees of freedom, while leaving the slow components of the dynamics unaffected. In fact, methods have been devised that implement this concept, based on approximate knowledge of the vibrational patterns associated with fast molecular motion [51]. Coloured-noise dynamics can also be used to this aim, with the considerable advantage that no prior knowledge of the dynamics is needed, and that one can simply specify a cutoff frequency below which the GLE dynamics aims at disturbing minimally the system's dynamics. In Ref. [12] it was shown that using this strategy it is possible to perform simulations of alanine dipeptide with a fully-flexible force field with an outer time step as large as 12 fs while slowing down the diffusive behaviour of ala_2 by less than 10%.

3 Non-equilibrium GLEs

Sampling configurations consistent with constant-temperature equilibrium conditions is perhaps the most straightforward application of our GLE framework. Eq. (10) is however considerably more general, and in principle one could very easily realise a stochastic dynamics for which $k_B T(\mathbf{A}_p + \mathbf{A}_p^T) \neq \mathbf{B}_p \mathbf{B}_p^T$, which does not satisfy the fluctuation-dissipation theorem and therefore does not guarantee sampling of the canonical ensemble.

A simulation based on this dynamics could be regarded as a model of the coupling of the physical system with several baths at different temperature, each coupled preferentially to different frequency ranges. In fact, one can exploit the possibility of solving the dynamics in the harmonic limit (and once more the invariance of a multi dimensional GLE to a unitary rotation of the coordinates) to predict the stationary distribution of a N-dimensional harmonic system in terms of a frequency-dependent effective temperature $T^\star(\omega)$. Furthermore, by fitting the parameters in $\mathbf{A}_p$ and $\mathbf{B}_p$ one can tune the fluctuations $\omega^2 \left\langle q^2 \right\rangle(\omega)$ and $\left\langle p^2 \right\rangle(\omega)$ to obtain the desired frequency dependence, leading to a number of useful effects.

3.1 δ-thermostat and f-thermostat

Perhaps, the simplest example of a "non-equilibrium" GLE is one that enforces a δ-like dependency of the effective temperature as a function of frequency [52]. In a harmonic system, this GLE will set a narrow range of frequencies to a finite effective temperature, and all other normal modes to a near-zero $T^\star$. Figure 8 shows the effect of applying δ-thermostats targeting different frequencies ω_0 to a quasi-harmonic system, namely an empirical force field model of ice. Despite the anharmonicity of the system, the dynamics does automatically excite the normal modes corresponding to the desired target. Once more, note that no information on the intrinsic vibrations of the system is used, and that the GLEs are integrated in the Cartesian basis.

An interesting – albeit not directly relevant to *ab initio* molecular dynamics – application of δ

Figure 8: Velocity-velocity correlation spectra for a flexible ice model [39], computed out of a series of simulations using δ-thermostats targeted at different frequencies ω_0.

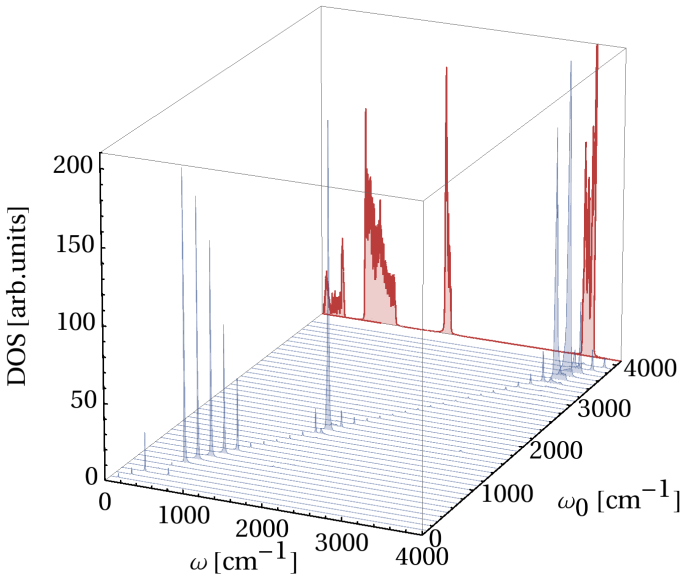

thermostats is the (approximate) evaluation of the density of states of a positive-definite matrix $\mathbf{M}$. The idea is to use $\mathbf{M}$ to define the quadratic potential of an artificial harmonic dynamics. When δ-thermostats centred on different frequencies ω are used on top of such potential, the mean kinetic energy obtained from the trajectory can be related to the density of states in the vicinity of $\epsilon = \omega^2$. This concept can be generalized to construct an f-thermostat [53], which can be used to evaluate selected elements of positive functions of positive-definite matrices. In practice one designs a GLE that enforces ω-dependent fluctuations of momentum that are related to the target matrix function f by $\langle p^2 \rangle (\omega) = f(\omega^2)$. Then, thanks to the rotational invariance of GLE dynamics one sees that, even though the artificial dynamics is *not* performed in the basis of the eigenvalues of $\mathbf{M}$, and in fact there is no explicit knowledge of the spectrum of the matrix, it will be true that $\langle \mathbf{p}\mathbf{p}^T \rangle = f(\mathbf{M})$. If $\mathbf{M}$ is sparse, the dynamics can be propagated with linear scaling effort, and so selected elements of $f(\mathbf{M})$ can be computed with linear complexity, avoiding the diagonalisation of $\mathbf{M}$.

3.2 The quantum thermostat

The methods discussed this far demonstrate nicely the effects that can be obtained by using GLEs that do not fulfil the fluctuation-dissipation relation between friction and noise memory kernels. Furthermore, they suggest a possible application to the evaluation of physical effects by *ab initio* molecular dynamics, beyond conventional Boltzmann sampling.

Consider a harmonic oscillator of frequency ω, sampled canonically at inverse temperature $\beta = 1/k_B T$. Its phase-space distributions for position and momentum are Gaussians $\rho(p) \propto \exp -p^2/2\sigma_p^2$ and $\rho(q) \propto \exp -q^2/2\sigma_q^2$, regardless of whether the oscillator is described classically or according to quantum mechanics. The classical and quantum cases only differ for the mean fluctuations: for a classical oscillator $\sigma_p^2 = m/\beta$ and $\sigma_q^2 = 1/\beta m\omega^2$, while for a quantum

Figure 9: Panel b) shows the expectation values of potential, kinetic and total energy for a proton in a 1D quartic double-well potential with minima separated by 1Å, as a function of the height of the barrier. Dotted lines correspond to reference quantum mechanical results, the continuous blue line corresponds to the classical mean total energy, and the red dots are the average values obtained from a quantum-thermostat simulation. As shown in panel a), the different barrier heights span different regimes, going from a quasi-classical limit for small barriers, to strongly quantised but quasi-harmonic conditions at very high barriers, with an intermediate regime in which tunnelling is non-negligible.

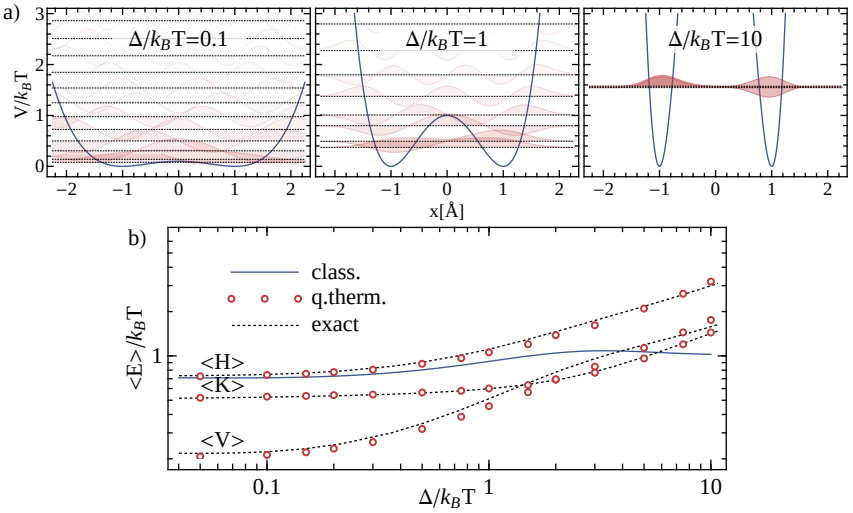

oscillator $\sigma_p^2 = m\frac{\hbar\omega}{2}\coth\frac{\beta\hbar\omega}{2}$ and $\sigma_q^2 = \frac{\hbar}{2m\omega}\coth\frac{\beta\hbar\omega}{2}$. One sees that quantum fluctuations at temperature T correspond to the fluctuations of a classical oscillator at the effective temperature

$$T^\star(\omega) = \frac{\langle p^2\rangle}{mk_B} = \frac{m\langle q^2\rangle}{k_B} = \frac{\hbar\omega}{2k_B}\coth\frac{\hbar\omega}{2k_BT}. \tag{13}$$

If one could perform a simulation of a compound in which different normal modes are thermalised at the effective, frequency-dependent temperature $T^\star(\omega)$, then the phase-space distribution and thermodynamic properties of the system would correspond to the distinguishable-particles quantum description of the nuclear degrees of freedom – at least in the harmonic limit. To achieve this while using conventional thermostatting, one would need to know the normal modes frequencies and phonon displacement patterns, and apply tailored white-noise thermostats at different temperatures working in the normal modes representation. GLE thermostatting, on the other hand, makes it possible to obtain the desired distribution without the need of knowing the normal modes of the system being studied: one only needs to fit a set of parameters that enforces the quantum fluctuations for any frequency within a range that encompasses the vibrational modes relevant for the system at hand, and then apply the same GLE to each Cartesian degree of freedom. The quantum $T^\star(\omega)$ is then enforced automatically, giving quantum fluctuations at the cost of conventional molecular dynamics.

This "quantum thermostat" (QT) idea [9, 13] works surprisingly well also for strongly anharmonic potentials (Figure 9). In fact, the main limitation when applying it to real systems does not depend much on failure to describe strongly anharmonic behaviour, but rather on the consequences of weak anharmonic coupling in a multi-dimensional system, giving rise to zero-point

energy leakage [9]. In practice the quantum thermostat tries to keep normal modes of different frequencies at different temperatures, and so in the presence of anharmonic coupling energy will tend to flow from high-frequency/high-temperature to low-frequency/classical temperature modes. This energy flow was not accounted for when designing $T^\star(\omega)$, and so there will be a (significant) deviation between the desired quasi-harmonic quantum fluctuations and the actual fluctuations.

This is a common problem in semi-classical methods to treat quantum nuclear effects [54], and has been also recognized in other stochastic approaches to obtain approximate quantum effects [55, 56]. Rather than trying to remedy this problem by exploiting information on the anharmonic couplings – which would be an ad-hoc, non-transferable solution, requiring in-depth knowledge of the system – we tried to control zero-point energy leakage by exploiting the tunability of the GLE thermostats, enforcing a strong coupling across the whole frequency range so as to counterbalance effectively the zero-point energy leakage. This approach improves significantly the performance of the quantum thermostat when applied to anharmonic problems [8, 9], and made it possible to describe qualitatively the role of NQEs in several real applications, as will be discussed further below.

However, the approximations behind the quantum thermostat and related semi-classical methods are basically uncontrolled, and very hard to gauge unless it is possible to perform a harmonic analysis – which in many ways defeats the purpose of applying these techniques in the first place. So, the quantum thermostat can be regarded as an inexpensive technique to assess qualitatively the importance of NQEs, but we would not recommend it to infer quantitative conclusions. However, coloured-noise is not only useful for approximate calculations: it can be used together with path integral molecular dynamics to obtain a systematically (and quickly!) converging method to quantitatively evaluate nuclear quantum effects, as will be discussed in the next section.

4 Combining path integral molecular dynamics and GLEs

The state-of-the art technique to describe the quantum nature of light nuclei exploits the path integral formalism [57], which maps the quantum mechanical partition function for a system of N distinguishable particles onto the *classical* partition function of a so-called ring polymer, composed of P replicas (beads) of the physical system and described by the Hamiltonian

$$H_P(\mathbf{p},\mathbf{q}) = \sum_{i=0}^{P-1} \frac{1}{2}\mathbf{p}_i^2 + V(\mathbf{q}_i) + \frac{1}{2}\omega_P^2 (\mathbf{q}_i - \mathbf{q}_{i+1})^2 , \tag{14}$$

where $\mathbf{q}_i$ and $\mathbf{p}_i$ are $3N$-dimensional vectors describing the mass-scaled positions and momenta of the particles in the i-th replica, and $V(\mathbf{q}_i)$ is the physical potential acting on replica i. The harmonic interaction between neighbouring beads is characterized by the frequency $\omega_P = P/\beta\hbar$, for a simulation at inverse temperature β. The ring polymer Hamiltonian (14) must be sampled at P times the physical temperature.

Averages of appropriate estimators computed over the ring-polymer canonical distribution will converge to the corresponding quantum mechanical expectation value as the number of replicas is

Figure 10: The frequency-dependent temperature (expressed as $g_P(x) = T^*(2x/\beta\hbar)/PT$, with $x = \beta\hbar\omega/2$) for the PI+GLE technique using different numbers of beads.

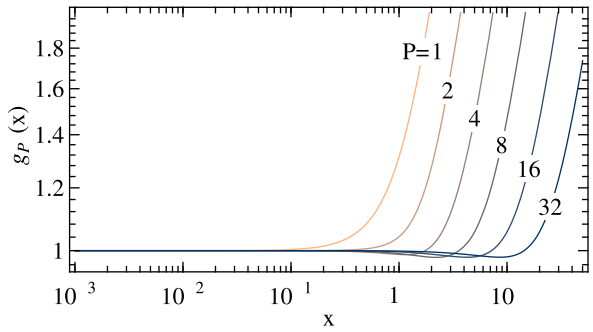

increased. For instance, the path integral estimator for the potential is just the mean (physical) potential of individual beads:

$$\langle V \rangle = \frac{1}{P} \sum_{i=0}^{P-1} \langle V(\mathbf{q}_i) \rangle \,, \tag{15}$$

whereas momentum-dependent properties typically require more complex estimators, e.g. the centroid-virial estimator for the kinetic energy

$$\langle K \rangle = \frac{3N}{2\beta} + \frac{1}{2P} \sum_{i=0}^{P-1} \langle (\mathbf{q}_i - \bar{\mathbf{q}}) \cdot \nabla V(\mathbf{q}_i) \rangle \,, \tag{16}$$

where $\bar{\mathbf{q}} = \sum_i \mathbf{q}_i / P$ is the centroid. The number of replicas needed to converge the value of these estimators is typically a small multiple of $\beta\hbar\omega_{\max}$, where $\omega_{\max}$ is the highest physical frequency present. This means for instance that including NQEs in liquid water at room temperature requires at least 32 replicas – a huge computational overhead that is not compensated by more efficient sampling as the different beads are strongly correlated with one another.

From the point of view of integrating the equation of motion, thermostatting [11], and what follows, it is useful to write the dynamics in terms of the normal modes of the free ring polymer. The harmonic part of the potential in (14) can be easily diagonalized, yielding the transformation between Cartesian coordinates $\mathbf{q}_i$ and normal-modes coordinates $\tilde{\mathbf{q}}_k$ (see e.g. Ref. [11]). The k-th normal mode will have, in the absence of an external potential, frequency $\omega_k = 2\omega_P \sin k\pi/P$.

4.1 Accelerating the convergence of configurational properties: PI+GLE

The quantum thermostat yields exact (apart from the very small errors in the fit of $T^\star(\omega)$) quantum fluctuations in the harmonic limit, but exhibits uncontrolled errors in real, anharmonic problems. Path integral molecular dynamics (PIMD) on the contrary can be converged systematically, but involve a very large computational overhead that is largely due to the high-frequency, strongly quantised vibrations, that are typically very close to harmonic. One is then led to wonder whether a hybrid technique, combining PIMD and correlated noise, could help achieve faster convergence while still allowing for quantitative accuracy and controlled error.

The crux is designing a GLE thermostat that enforces exact quantum fluctuations in the harmonic limit *for any number of replicas*, even in cases where PIMD alone would be far from converged. Then, such a PI+GLE method would be always exact for harmonic problems, and

Figure 11: Probability density for a hydrogen atom in a quartic double-well potential with the minima separated by 0.6Å and a barrier height of 1000K. All simulations were performed with a target temperature of 300 K. The exact quantum mechanical result (dashed black line) was obtained by numerical solution of the Schrödinger equation, the contributions of the various eigenstates being averaged with the appropriate Boltzmann weight. The four panels compare this exact result with the PIMD (blue line) and PI+GLE (red line) results with increasing bead numbers.

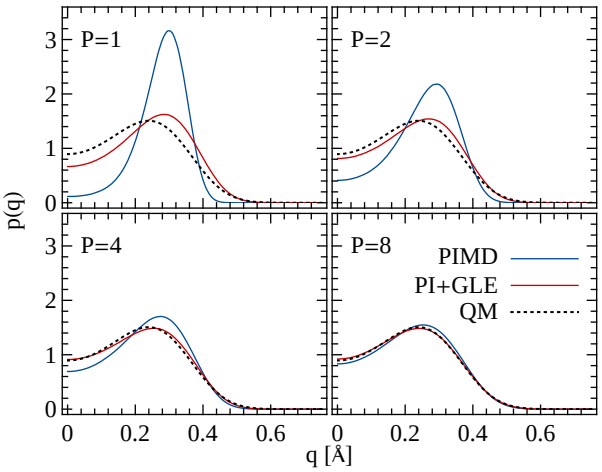

naturally converge to (Boltzmann-sampled) PIMD when the number of beads is large enough to have a converged result in the absence of correlated noise.

In order to work out the properties of the GLE that would achieve this goal, one can proceed in the same way as with the quantum thermostat, only considering that now, in the presence of a harmonic potential of frequency ω, the dynamics will be characterised by frequencies $\omega_k = \sqrt{\omega^2 + 4P^2 \sin^2 k\pi/P}$. These are the frequencies that will be picked up by the colored-noise dynamics, so, introducing a frequency-dependent *configurational* temperature $T^*(\omega) = \langle q^2 \rangle (\omega) m\omega^2/k_B$ (momentum fluctuations are not important per se in a PIMD framework), one gets the requirement for having quantum fluctuations of the beads to be

$$\frac{m\omega^2}{k_B T}\langle q^2 \rangle = \frac{m\omega^2}{Pk_B T}\sum_i \langle q_i^2 \rangle = \frac{m\omega^2}{Pk_B T}\sum_k \langle \tilde{q}_k^2 \rangle = \frac{1}{P}\sum_k \frac{T^*(\omega_k)/T}{\omega_k^2/\omega^2} = \frac{\hbar\omega}{2k_B T}\coth\frac{\hbar\omega}{2k_B T}. \quad (17)$$

Since ω_k depends on the physical frequency ω, Eq. (17) must be seen as a functional equation that defines the $T^*(\omega)$ curve – if any – that satisfies it for any oscillator frequency ω. In Ref.[14] it is discussed how to numerically solve this functional equation, and the resulting target $T^*(\omega)$ for different number of beads are provided in the supporting information of the same reference. Note incidentally that it is essential that one can tell precisely what will be the ring-polymer dynamics in a harmonic potential: the discussion should be modified if one used anything other than the physical masses for the normal modes propagation.

Figure 10 shows the frequency-dependent effective temperature relative to the temperature PT that would be used in a conventional PIMD simulation, as a function of the number of replicas. As the number of replicas increases, the curve is just equal to one up to larger and larger "quantumness" parameter $x = \beta\hbar\omega/2$. For a given frequency and temperature, as the number of beads is increased, PI+GLE will behave more and more as a conventional PIMD with Boltzmann

Figure 12: The average value of the potential energy, the virial kinetic energy and the constant-volume heat capacity for a simulation of a flexible water model [39] at T = 298 K, plotted as a function of the number of beads. The results obtained with conventional PIMD and PI+GLE are compared, and the value of V obtained with the original quantum thermostat10 (QT) is also reported.

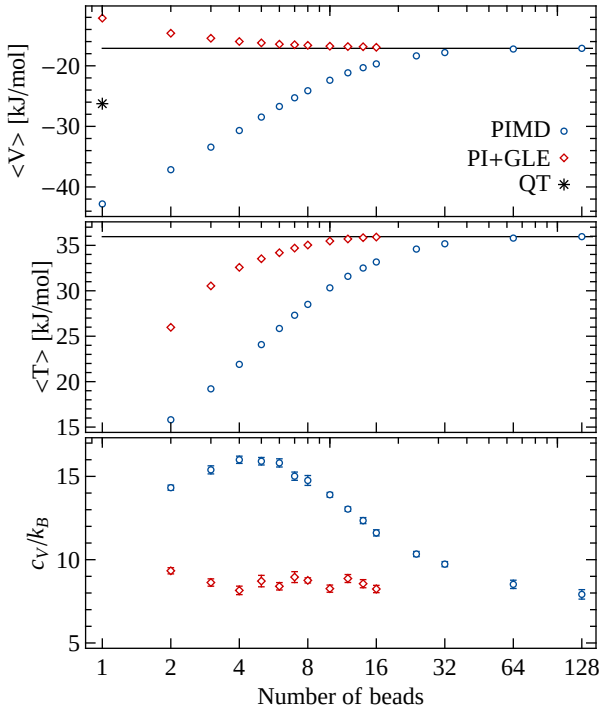

sampling of the ring-polymer Hamiltonian. This implies that PI+GLE is bound to converge to the exact quantum averages, just because in the large P limit it converges to PIMD. As shown in Fig. 11, even for a strongly anharmonic quantum problem, the convergence is considerably accelerated.

Furthermore, PI+GLE makes it possible to systematically converge results also in the case of real, anharmonic multidimensional problems. As the number of replicas is increased, the $T^*(\omega)$ curve becomes flatter and flatter, and so there is a less pronounced effective temperature gradient between the high and low frequency modes, so zero-point energy leakage (using here the term in a loose sense) is a lesser concern than in the case of the quantum thermostat. Even though it is still important to enforce effective coupling to the thermostat, one can avoid the strong overdamping that must be used with the quantum thermostat, with considerable advantages in terms of sampling efficiency for for the slow, diffusion-like modes.

Figure 12 shows the convergence with number of beads of potential and kinetic energy for a quantum simulation of an empirical water model [39] at room temperature, comparing plain PIMD and PI+GLE. Colored noise accelerates dramatically the convergence of observables to the quantum expectation values, and the possibility of converging results systematically makes it possible to assess the error. A careful examination of Figure 12 shows that the mean kinetic energy $\langle T \rangle$ converges somewhat more slowly than $\langle V \rangle$. This is due to a specific shortcoming of PI+GLE, that will be addressed in the next section.

4.2 Including imaginary-time correlations: PIGLET

As noted above, when using PI+GLE the quantum kinetic energy seems to converge more slowly than the average potential, or other structural quantities such as radial distribution functions. If one considers carefully the expression for the kinetic energy estimator (16) in the harmonic limit, it becomes apparent why:

$$\begin{aligned}\langle T\rangle =&\frac{1}{2\beta}+\frac{1}{2P}\omega^2\sum_{i=0}^{P-1}\left\langle q_i^2\right\rangle-\frac{1}{2}\omega^2\left\langle\bar{q}^2\right\rangle= \\ =&\langle V\rangle+\frac{1}{2\beta}-\frac{1}{2}\omega^2\left\langle\bar{q}^2\right\rangle.\end{aligned} \tag{18}$$

In a quantum mechanical description, the average potential and kinetic energy of a harmonic oscillator of frequency ω read

$$\langle V\rangle=\langle T\rangle=\frac{\hbar\omega}{4}\coth\frac{\beta\hbar\omega}{2}. \tag{19}$$

In order to obtain the correct quantum value for $\langle T\rangle$, it is not sufficient to design the GLE so that the fluctuations of q are consistent with $\langle V\rangle=\frac{\hbar\omega}{4}\coth\frac{\beta\hbar\omega}{2}$, but it is also necessary to make sure that $\frac{1}{2}\omega^2\left\langle\bar{q}^2\right\rangle=\frac{1}{2\beta}$.

This points at a general limitation of the basic PI+GLE idea: only the "marginal" distribution of the beads is bound to be exact in the harmonic limit, which warrants accelerated convergence of any observable that depends only on q but does not necessarily help converging more complex estimators that also depend on the correlations between different beads. Fortunately, it is relatively easy to extend the PI+GLE idea to include further correlations. In fact, PIMD can be very effectively propagated in the free-particle normal modes representation, i.e. by transforming the coordinates to $(\tilde{q}_k,\tilde{p}_k)$ and writing the equations of motion in that base [11]. The physical potential acts in the same way on all the beads, so in the harmonic limit it only amounts to a diagonal perturbation of the free ring polymer, that changes the vibrational frequencies as discussed above, but does not change the eigenvectors. Hence, in a multi-dimensional context it is possible to transform individual degrees of freedom in the *free particle* normal modes representation, without the need to diagonalise the physical potential, and it is possible to apply GLEs with different temperature curves $T_k^*(\omega)$ onto different *free particle* coordinates. In practice, this makes it possible to enforce multiple constraints on the distribution of the ring polymer, including bead-bead correlations as well as the marginal distribution that guarantees fast convergence of structural properties.

Let us elaborate on this idea, focussing on the objective of accelerating the convergence of the centroid-virial kinetic energy estimator. Eqs. (18) and (19) clearly require that the centroid must be distributed classically, so $T_0^*(\omega)=PT$, as in conventional PIMD. There is then just one more condition to be enforced, namely the marginal distribution of the q_is, which now has to be determined knowing that the centroid is distributed classically:

$$\frac{m\omega^2}{Pk_BT}\sum_k\left\langle\tilde{q}_k^2\right\rangle=1+\frac{1}{P}\sum_{k>0}\frac{T^*(\omega_k)/T}{\omega_k^2/\omega^2}=\frac{\hbar\omega}{2k_BT}\coth\frac{\hbar\omega}{2k_BT}. \tag{20}$$

This functional equation can be solved similarly to Eq. (17), now singling out the $k=1$ term to devise a fixed-point iteration that converges to the desired, universal $T^*(\omega)$ curve.

Figure 13: The quantum contribution to the potential energy, and to the kinetic energy of hydrogen and oxygen atoms as computed by the centroid virial estimator for a simulation of a flexible water model [39] at T = 298 K, plotted as a function of the number of beads. Note the much accelerated convergence rate of the kinetic energy when using PIGLET compared to PI+GLE.

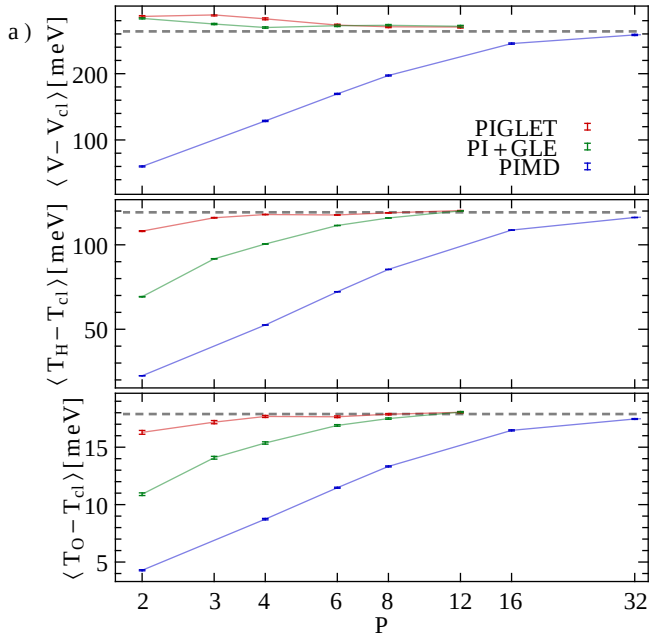

Figure 13 shows clearly that PIGLET is considerably more efficient than PI+GLE in converging the quantum kinetic energy of atoms, even for an anharmonic problem such as liquid water. The convergence of structural properties for the two methods is very similar, highlighting the fact that it is possible to manipulate bead-bead correlations without disrupting the efficient convergence of the marginal distribution of individual beads.

The centroid-virial estimator does not exhaust the list of physical observables that depend on bead-bead correlations: imaginary-time correlation functions provide moment constraints that can be used to improve the reliability of real-time approximate quantum dynamics [58, 59], scaled-coordinate estimators make it possible to obtain directly the heat capacity [60], displaced path estimators can be used to compute the particle momentum distribution [61], and free-energy perturbation estimators give access to isotope fractionation ratios [62]. In all of these cases one could try to figure out which constraints ought to be enforced on the ring polymer distribution to obtain exact expectation values in the harmonic case, and use them to determine a number of $T_k^*(\omega)$ curves to be used to design GLEs for the different ring-polymer normal modes.

In some cases it is possible that a given combination of PIMD and GLEs accelerates convergence of estimators it has not been designed specifically for. For instance, PI+GLE does yield faster convergence of the centroid-virial kinetic energy (albeit not as fast as PIGLET), and PIGLET appears to speed up the convergence of the "thermodynamic" free-energy perturbation estimator of isotope fractionation [62]. The possibility of obtaining systematic convergence by increasing the number of beads means one can empirically assess the accuracy for a given estimator and physical problem by performing test simulations with increasing number of beads, much like one would converge a plane waves cutoff, a k-points mesh, or conventional PIMD.

In principle, one could also try to combine GLE thermostatting with high-order path integration [63–65], in an attempt to further reduce the number of replicas needed to achieve convergence. The unfavourable system-size scaling of the re-weighting procedure that is needed for most high-order PIMD schemes [66] suggests that such method would be beneficial only for simulations including a small number of atoms, which is often the case in *ab initio* applications.

5 Implementation and usage

One of the advantages of the GLE framework that is discussed here is that it allows one to achieve a variety of useful effects within the very same formalism, so that from the point of view of implementation a relatively simple change to the code is sufficient to make available all the different shades of colored-noise thermostats.

5.1 Symmetric-split propagator

Implementing an integrator for a GLE thermostat is relatively simple thanks to the linear nature of the stochastic differential equations (10). At variance with thermostats based on second-order equations of motion such as Nosé-Hoover, where a multiple time-step approach is required to obtain accurate trajectories [67, 68], GLE thermostats can be readily introduced on top of a velocity-Verlet integrator. In the symmetric Trotter split form [46], propagation of p and q across a finite time step Δt can be written as

$$\begin{aligned} p \leftarrow & p + V'(q)\Delta t/2 \\ q \leftarrow & q + p\Delta t/m \\ p \leftarrow & p + V'(q)\Delta t/2. \end{aligned} \tag{21}$$

Eqs. (21) can be obtained using Trotter splitting in a Liouville operator description of the dynamics. A thermostat can be introduced on top of this scheme by performing two free-particle steps by $\Delta t/2$ on the $(p, \mathbf{s})$ variables[69]:

$$\begin{aligned} (p, \mathbf{s}) &\leftarrow \mathcal{P}\left[(p, \mathbf{s}), \Delta t/2\right] \\ p &\leftarrow p + V'(q)\Delta t/2 \\ q &\leftarrow q + p\Delta t/m \\ p &\leftarrow p + V'(q)\Delta t/2 \\ (p, \mathbf{s}) &\leftarrow \mathcal{P}\left[(p, \mathbf{s}), \Delta t/2\right]. \end{aligned} \tag{22}$$

The finite-time step for $(p, \mathbf{s})$, in the absence of an external potential, can be readily obtained as:

$$\mathcal{P}\left[(p, \mathbf{s}), \Delta t\right]^T = \mathbf{T}(\Delta t)\,(p, \mathbf{s})^T + \sqrt{m}\mathbf{S}(\Delta t)\boldsymbol{\xi}^T \tag{23}$$

where $\boldsymbol{\xi}$ is a vector of $n+1$ uncorrelated Gaussian numbers, and the matrices $\mathbf{T}$ and $\mathbf{S}$ can be computed once,[2] at the beginning of the simulation and for all degrees of freedom[26, 70]. The

[2]Note that in many cases $\mathbf{S}\mathbf{S}^T$ is ill-conditioned, and so a Cholesky decomposition may fail to yield $\mathbf{S}$. In a GLE implementation it is better to compute $\mathbf{S}$ by means of a LDL^T decomposition, or even better to just diagonalise $\mathbf{S}\mathbf{S}^T$ and compute the symmetric square root: tiny, negative eigenvalues that can occasionally appear can then be safely set to zero.

relations between $\mathbf{T}$, $\mathbf{S}$, $\mathbf{A}_p$, $\mathbf{C}_p$ and Δt read

$$\mathbf{T} = e^{-\Delta t \mathbf{A}_p}, \mathbf{S}\mathbf{S}^T = \mathbf{C}_p - e^{-\Delta t \mathbf{A}_p}\mathbf{C}_p e^{-\Delta t \mathbf{A}_p^T}.$$

When the GLE samples the canonical ensemble, $\mathbf{C}_p = k_B T$ and the fluctuation-dissipation theorem holds, the Boltzmann distribution is invariant under the action of (23), whatever the size of the time-step. A useful consequence of this property is that, in the rare cases where applying (23) introduces a significant overhead over the force calculation, the thermostat can be applied every M steps of dynamics, using a stride of M Δt. This will change the trajectory, but does not affect the accuracy of sampling. When using a non-canonical thermostat, instead, accurate integration of the GLE is crucial to obtain the desired frequency-dependent stationary distribution, and so one must pay more attention to the time step.

The velocity-Verlet algorithm (21) introduces finite-Δt errors, whose effect needs to be monitored. In microcanonical simulations, this is routinely done by checking conservation of the total energy H. Following the work of Bussi *et al.* [24] we introduce a conserved quantity $\tilde{H}$, which can be used to the same purpose:

$$\tilde{H} = H - \sum_i \Delta K_i \tag{24}$$

where ΔK_i is the change in kinetic energy due to the action of the thermostat at the i-th time-step, and the sum is extended over the past trajectory. This strategy can be applied to both the canonical and non-canonical GLEs, but only in the former case the conservation of $\tilde{H}$ can be rigorously considered as a measure of how well detailed balance is satisfied. For "non-equilibrium" GLEs, the conservation of $\tilde{H}$ should only regarded as a sign that the Hamiltonian part of the dynamics uses a sufficiently small time step. Furthermore, it is worth noting that strict fulfilment of detailed balance is a sufficient but non necessary condition to attain canonical sampling. In many cases, for instance when using a GLE to stabilize multiple-time step dynamics [12], it is normal for $\tilde{H}$ to drift considerably as the thermostat is actively counteracting the integration errors that would lead to unstable dynamics. Nevertheless, one can verify that in this and other cases the efficient sampling that is enforced by a well-tuned GLE guarantees that integration errors do not add up, and that the sampled ensemble stays very close to the desired one. This can be exceedingly useful in *ab initio* simulations, where an effective thermostatting strategy can enable the usage of larger time steps, or make it possible to obtain reliable statistical averages from molecular dynamics performed with noisy, poorly converged forces [71].

5.2 Obtaining GLE parameters

Since the implementation of a GLE dynamics is relatively straightforward, as discussed in the previous paragraph, the main issue is how to design a set of parameters that yields the best performance for a given application. The formalism is very general, and so even with a small size of the extended phase-space vector $\mathbf{s}$, the drift matrix $\mathbf{A}_p$ contains tens of parameters that in principle could be varied independently. It would therefore be completely impractical to optimise the thermostat by performing actual simulations on the system of interest: the usefulness of this GLE framework rests entirely on the possibility of designing the thermostat *a priori*, based on superficial knowledge of the problem at hand and a profound understanding of the general sampling issues that may be critical to address.

For instance, the "smart sampling" procedure described in Section 2.1 only relies on knowledge of the highest frequency present in the system (which is also determining the time step), and of a rough estimate of the affordable simulation time (which determines which is the slowest process that can be studied by unbiassed dynamics). Then, the optimization of the GLE parameters can be accomplished by just optimising a proxy of the sampling efficiency (e.g. the correlation time of the potential energy) using analytical estimates that are exact in the harmonic limit. In some cases [10, 12] it might also be possible to write a simplified $\mathbf{A}_p$ that depends on a small number of physically meaningful parameters.

Either way, the fact that optimised sets of parameters are obtained based on general considerations means that they can be easily transferred from one system to another, exploiting simple scaling rules that make it possible to change the target frequency range or temperature [8, 9]. In a way, the generation and the use of GLE parameters shares many similarities with the case of pseudopotentials – that are obtained by a non-trivial procedure but can then be transferably applied seamlessly to many different problems. To simplify the task of choosing the correct GLE parameters, an on-line repository has been prepared [72], from which $\mathbf{A}_p$ and $\mathbf{C}_p$ matrices optimized for the different flavours of GLE thermostatting can be retrieved, scaled to the relevant frequency range and converted to the desired units or even to the input format of the desired simulation software, if it possesses a native GLE implementation.

5.3 Running path integral simulations

The fact that classical momenta are immaterial within the imaginary-time path integral formalism implies that different choices of masses have been taken to integrate effectively the equations of motion, which are nicely summarized for instance in Ref. [73]. Not many electronic structure codes implement PIMD, and they often make different choices in terms of the integration strategy and the mass scaling. PI+GLE and its generalizations rely on a precise relation between the dynamical frequencies of the ring polymer and its configurational fluctuations, which implies that different $T^*(\omega)$ curves – and consequently GLE parameters – would need to be devised for each choice of masses. To avoid this complication, and to reduce the implementation burden of bringing imaginary time PIMD to the codes that do not provide this functionality yet, we have developed i-PI, a Python interface for (*ab initio*) (path integrals) molecular dynamics [72, 74].

Even though it can be used in principle also with empirical force fields, i-PI has been developed with *ab initio* simulations in mind. Whenever the electronic structure problem is solved explicitly, the cost of the simulation will be dominated by the evaluation of the forces, and so i-PI had been designed to be reasonably efficient, but not at the cost of clarity. The effort required to modify the *ab initio* electronic structure code is kept to a minimum using a client-server model, where the i-PI server and the *ab initio* client are run separately and communicate through sockets (see Figure 14). The server has an xml-formatted input, that defines the options of the ionic dynamics, including if desired GLE parameters, and the initial configurations of the atoms and the simulation cell. When started, it listens on the specified port and network interface (or UNIX domain socket), waiting for clients to connect. The client reads its own input file, that specifies all the parameters of the electronic structure calculations as well as the number and type of atoms present in the simulation. The only requirement is that the internal order of atoms

Figure 14: Schematic overview of the client-server model underlying i-PI. The communication is kept to a minimum, and so are the modifications that need to be made to adapt an existing electronic structure code to act as the client. The client is not restarted between successive force evaluations, so as to avoid the overhead associated with initialisation.

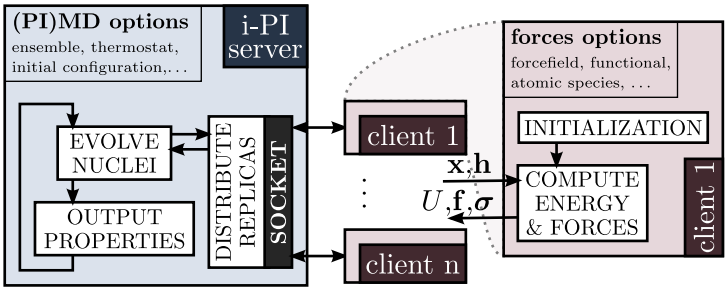

matches the order in the input of i-PI. Then, it connects to the server, which maintains a list of active clients. When i-PI needs energy and forces to propagate the dynamics, it dispatches atomic configurations to the active clients, that use them to perform an electronic structure optimisation and return energy, forces, and the potential energy part of the pressure tensor.

This architecture avoids the initialization overhead – as the client stays active in between successive force evaluations – and makes it easy to use optimizations such as the extrapolation of the wavefunction within the *ab initio* client. In the case of path integral simulations, different replicas can be computed simultaneously by separate clients, so the trivial level of parallelism inherent in PIMD can be fully exploited. i-PI has a modular structure, it implements advanced features such as PIMD and PIGLET in the constant-pressure ensemble, scaled-coordinates estimators, etc. and can be easily extended. Interfaces to several electronic structure codes (including CPMD[75], CP2K[76], quantum-Espresso[77], FHI-AIMS[78]) are either included in the development version of the code, or available as patches.

6 Applications

Having discussed the theoretical foundations, the methodological details, and the practical implementation of the GLE thermostat framework, let us now briefly describe a few representative applications that demonstrate how it can be used in the context of *ab initio* molecular dynamics.

6.1 Structural disorder in lithium imide

As discussed in Section 1, the "efficient sampling" aspects of GLE thermostatting are best tested using inexpensive empirical potentials, as has been done for instance in Section 2.1 of the present review. Assessing the statistical efficiency of a simulation in a quantitative, objective way implies computing accurate autocorrelation times, which for non-trivial observables requires much too long to converge properly with *ab initio* MD, and so one ends up running time consuming tests that only produce anecdotal indications of the best sampling strategy.

With this caveat in mind, the study of Li_2NH in Ref. [80] can be regarded as an example in which optimal sampling GLE made it possible to investigate structural transition in a complex

Figure 15: (a) Tetrahedral arrangement of NH groups around a Li^+ vacancy in the low-temperature phase of lithium imide. (b) Li ions are distributed on the three symmetry unique sites, as labelled in the panel. The interstitial Li3 sites have fractional occupation. Sites which are left empty in the $Ima2$ model of Ref. [79] are shown as transparent spheres. (c) Occupied Li4 octahedral sites obtained upon relaxation of the $Ima2$ model. (d) A tetrahedral cluster of four interstitial ions at Li3 sites around a vacancy at the Li2 site, as obtained from a optimal-sampling MD starting from interstitials in the Li4 sites.

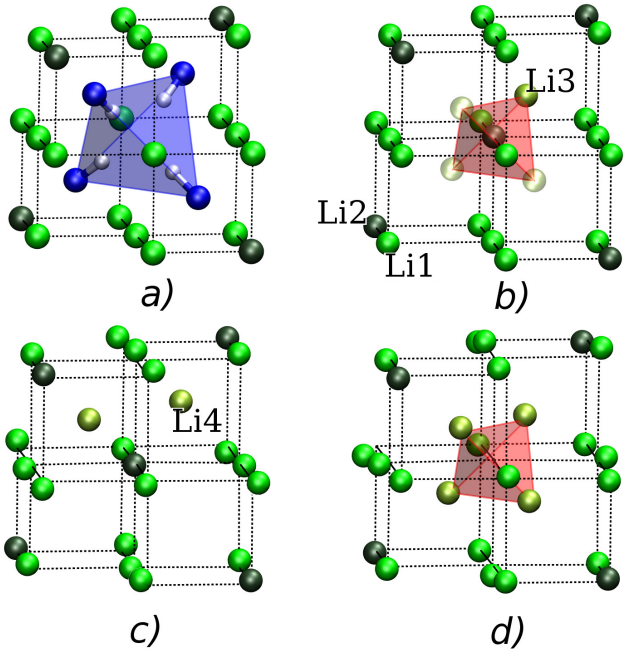

system within the time scale accessible to *ab initio* MD, without the need to resort to time consuming preliminary tests of the statistical efficiency of the dynamics. Lithium imide has a complex structure that can be understood in terms of a cubic lithium lattice with vacancies and interstitials, and with correlations between these defects and the orientation of NH groups in the structure (see Figure 15).

The distribution of vacancies and interstitials is partially disordered, and so diffraction experiments cannot determine the local ordering of defects that is important to understand the reactivity of the system, which is a candidate hydrogen-storage material. A simulation started from a proposed model of the structure lead to spontaneous diffusion of the interstitials and to the formation of vacancy-interstitial clusters that lower considerably the energy of the structure and led to better agreement with the diffraction data. It is worth mentioning that the same structure was simultaneously identified by high-throughput screening of the possible spinel-like structures of this compound [81]. When sampling phase space efficiently, molecular dynamics can be as effective as sophisticated search algorithms that are less generally applicable.

6.2 Particle momentum distribution in lithium imide

Lithium imide has also been the first system in which the quantum thermostat has been used together with first-principles MD to investigate the importance of nuclear quantum effects in hydrogen-containing materials [82]. Since the quantum thermostat and similar semi-classical methods can only provide a qualitative description of the quantum nature of nuclei, this study focused on the evaluation of the particle momentum distribution (PMD), a quantity that can be measured experimentally by deep inelastic neutron scattering [83], provides insight into the local environment of light atoms in complex environments [84] and differs dramatically from the classical, Maxwell-Boltzmann distribution. The disordered character, and the strongly anharmonic lattice dynamics of Li_2NH makes it questionable the use of a purely harmonic approximation to treat the quantum effects as it is often done in simpler crystalline materials [85, 86].

In a quantum thermostat framework it is very simple to compute particle momentum distributions, since the fluctuations of p are designed to reproduce the quantum mechanical ones in the harmonic limit. So – within the limits of the approximation – one can simply accumulate a histogram of the values of p observed in the course of the simulation. Figure 16 demonstrates the dramatic discrepancy between the experimental proton momentum distribution and that obtained from a classical simulation. The quantum thermostat improves dramatically the agreement with the experiment, even though the quantitative error is comparable to the one that could be expected from the use of harmonic lattice dynamics. The fact that the quantum thermostat cannot be converged systematically means that it is best used as an inexpensive assessment of whether NQEs play an important role in determining the value of an experimental observable, or can be safely ignored. It has for instance been used to this aim to study solid-state models of the solvated proton [87], the recombination of hydronium and hydroxide in water [88], and the graphite-diamond coexistence line [89]. In order to achieve quantitative accuracy, however, combination of the GLE with PIMD is essential.

Figure 16: The left panel compares the spherically-averaged PMD for hydrogen atoms in Li_2NH at 300K as obtained by deep inelastic neutron scattering experiments, with the theoretical results from a simulation with classical nuclei (which is just the Maxwell-Boltzmann distribution), from harmonic lattice dynamics and from molecular dynamics supplemented with a quantum thermostat. The right panel shows the three-dimensional PMD from the quantum thermostatted simulation, referenced to the crystalline axes. Note the anisotropy of the distribution, which is a clear, qualitative signature of quantum behaviour.

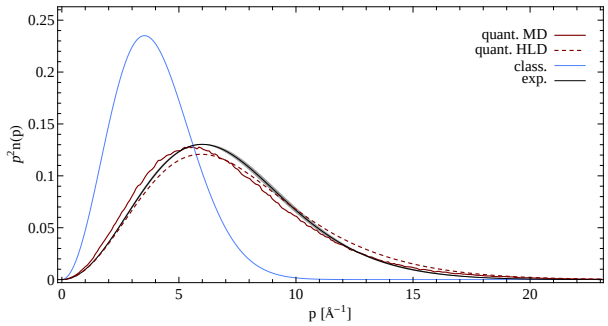

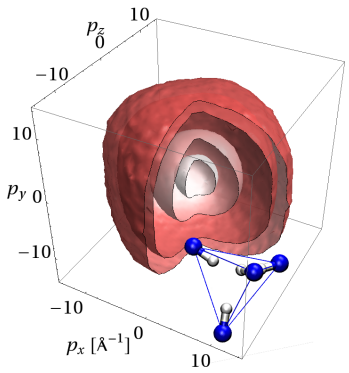

6.3 Competing quantum effects on the melting of heavy water

An example of a case in which it is necessary to obtain precise, quantitative results is the study of quantum effects on phase transitions. The quantum kinetic energy change upon phase transition can be related to the isotope effect on the transition temperature [90, 91]. By very simple arguments, one can infer that the deuteron kinetic energy change upon melting should be of the order of 0.5meV, which is tiny compared to the total kinetic energy – of the order of 100meV.

Path integral simulations have been suggesting for some time that quantum effects in water can be separated into different "components", that have opposite effects on many physical properties of H_2O, so that the net impact of NQEs is small even though each individual component is large [39, 92, 93]. Using PIGLET simulations of liquid and solid D_2O, and approximating the deuteron momentum distribution as an anisotropic Gaussian with principal values related to the NQEs along different molecular axes, it was possible to observe the partial cancellation that leads to a small overall change and ultimately explains why the melting temperatures of light and heavy water differ by just 4K. These findings qualitatively matched the experimental decomposition of the quantum kinetic energy change obtained by a neutron Compton scattering study of heavy water across the solid-liquid phase transition [94].

6.4 Nuclear quantum effects and hydrogen bond fluctuations in water

NQEs are typically much more pronounced when one looks at properties that depend on fluctuations – heat capacity or pH for example. The impact of NQEs is striking when one looks at the delocalisation of a proton along a hydrogen bond (HB) in water [95]. The proton transfer coordinate ν (the difference between the covalent O-H bond length and the distance between the hydrogen atom and the hydrogen bond acceptor O′) is a very effective order parameter to

Figure 17: (a) Distribution of the proton-transfer coordinate ν in *ab initio* simulations of water at 300 K. The three curves correspond to a classical simulation, to the distribution of the ring polymer beads in a simulation that includes quantum effects, and to the distribution of the centroid of the ring polymer in the quantum simulation. (b) Conditional average of the gyration radius of the ring polymer in the directions parallel ($r_{\parallel}$) and perpendicular ($r_{\perp}$) to the O-H covalent bond for different values of ν for the centroid.

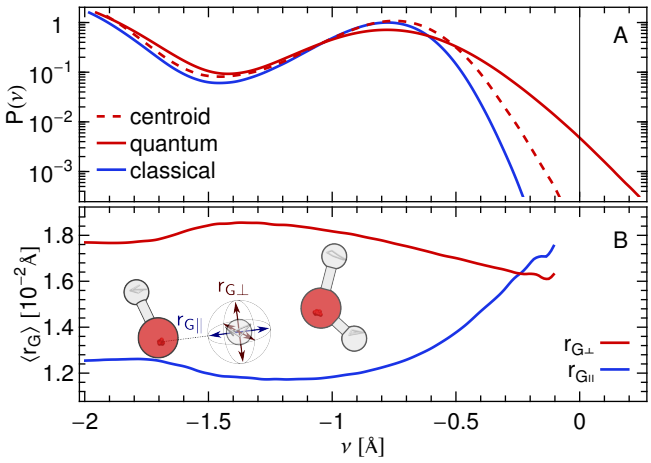

quantify the magnitude of the fluctuations. Figure 17a compares the probability distribution of ν in an *ab initio* simulation of water performed using classical MD, and treating the nuclei as quantum particles. Whereas in classical simulations there is only a negligible probability that a proton fluctuates up to $\nu = 0$, being half-way between the donor O and acceptor O′, in quantum simulations this probability increases by a factor of 10000. As shown in Figure 17b, this effect is due to the swelling of the ring polymer in the direction parallel to the hydrogen bond, that leads to transient autoprotolysis events accompanied by considerable rearrangements of the electron density.

In fact, this effect is observed to a much lesser extent in an empirical water model [39], even though a recent non-dissociable force field obtained by force-matching to first-principles simulations have been shown to be able to reproduce it quantitatively [96]. Density functional theory is known to exaggerate charge transfer, and so this result had to be validated by comparing different functionals, including dispersion corrections and hybrid functionals. The use of PIGLET made it possible to perform extensive tests, that showed that the magnitude of the effect is conserved to within a factor of two depending on the details of the electronic structure calculation. Also, it made it possible to gather extensive statistics (more than 50ps of quantum MD), which in turns allowed us to evaluate the correlations between proton excursions along consecutive hydrogen bonds (see Figure 18). The cooperative nature of these quantum fluctuations suggests that these effects may be magnified in situations in which the hydrogen bond network is distorted, as it may be the case at high pressures or in confinement.

In fact, simulations of water at high temperature and pressure (750K and 10GPa) [74] show a much larger fraction of water molecules with a (formal) net charge. Despite the high temperature, quantum nuclear effects still play a dramatic role in determining the fluctuation properties of the HB. A purely structural definition of charged species is somewhat ambiguous, considering the strong delocalization of protons. One can however estimate the presence of about 0.2% of

Figure 18: a) The joint probability distribution of the PT coordinate for the two hydrogen bonds donated by a tagged water molecule, $P(\nu_a, \nu_b)$. The lower-right corner shows the relative conditional probability $P(\nu_a, \nu_b)/P(\nu_a)P(\nu_b)$. b) The joint probability distribution $P(\nu_a, \nu_b)$ of the PT coordinate for one accepted and one donated HB for a given water molecule. The lower-right corner shows the relative conditional probability.

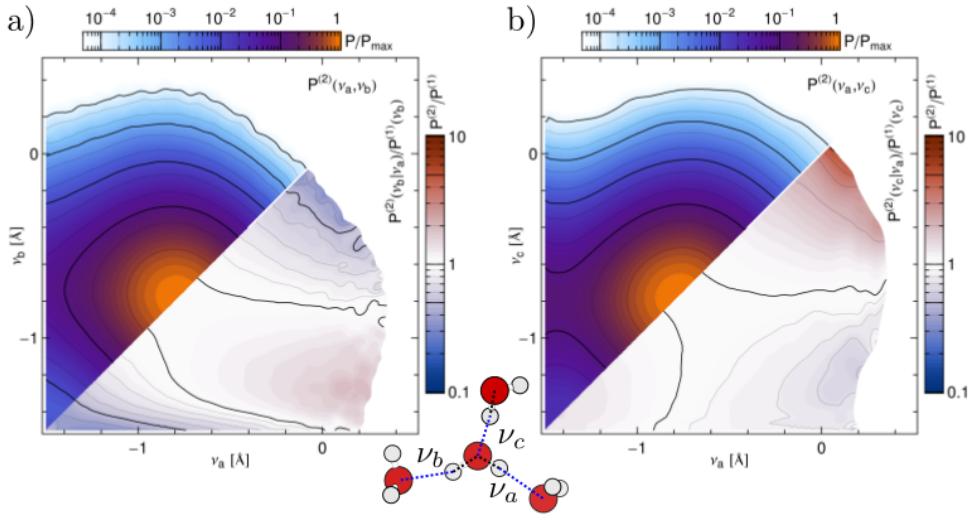

genuine autoionization events in the quantum simulations, that result in considerable exchange of protons between water molecules on the time scale (40ps) of the simulation. By comparison, no long-lived proton exchanges were observed in the corresponding classical run, and the fraction of "long-lived" inonized species was lower than 0.01%.

7 Outlook

Using a generalized Langevin equation as a sampling device, to manipulate the properties of molecular dynamics trajectories, has proven to be an exceedingly flexible tool. It allows one to enhance the efficiency of constant-temperature sampling as well as to reduce dramatically the cost of accounting for the quantum nature of light nuclei within atomistic models. These successes are due to the combination of 1) a very general formulation of the coloured-noise dynamics, 2) the possibility of predicting static and dynamical properties analytically in the harmonic limit, 3) the fact that the predictions for a 1D harmonic oscillator carry on to multi-dimensional problem even if the dynamics is integrated using the Cartesian coordinates, so that it is not necessary to know the vibrational modes of the system being studied.

GLE thermostats can be used transparently with any form of inter-atomic potential, but they are particularly useful in the case of *ab initio* simulations, where the high computational cost makes it a necessity to extract as much statistics as possible from short runs, and where it is almost impossible to benchmark the efficiency of different thermostats in a quantitative and objective way. Similar arguments can be made in favour of the use of GLEs to model nuclear quantum effects. NQEs can have a large impact on the accuracy of *ab initio* simulations in the presence of light atoms. At variance with empirical forcefields, that are fitted to experiments and therefore may account for the quantum nature of nuclei in an effective way, first-principles

MD uses the bare Born-Oppenheimer potential, and so completely neglects zero-point energy or tunnelling. The quantum thermostat provides a completely inexpensive strategy to qualitatively assess the importance of NQEs, and combinations of coloured noise and imaginary-time path integrals yield quantitative accuracy at a fraction of the cost of conventional PIMD.

As native implementations of GLE thermostats become available in more codes, and as the i-PI interface brings PI+GLE and PIGLET to any electronic-structure package with minimal effort, it will become easier to sample the configurations of complex materials and to fully account for the quantum nature of nuclei, extending even further the usefulness of *ab initio* MD for materials discovery and the understanding of chemical reactivity.

References

[1] K. Burke. Perspective on density functional theory. *J. Chem. Phys.*, 136(15):150901, 2012.

[2] M. Cococcioni and S. de Gironcoli. Linear response approach to the calculation of the effective interaction parameters in the LDA+U method. *Phys. Rev. B*, 71(3):035105, 2005.

[3] A. Tkatchenko and M. Scheffler. Accurate Molecular Van Der Waals Interactions from Ground-State Electron Density and Free-Atom Reference Data. *Phys. Rev. Lett.*, 102(7): 073005, 2009.

[4] S. Grimme, J. Antony, S. Ehrlich, and H. Krieg. A consistent and accurate ab initio parametrization of density functional dispersion correction (DFT-D) for the 94 elements H-Pu. *J. Chem. Phys.*, 132(15):154104, 2010.

[5] J. Klimeš and A. Michaelides. Perspective: Advances and challenges in treating van der Waals dispersion forces in density functional theory. *J. Chem. Phys.*, 137(12):120901, 2012.

[6] D. Frenkel and B. Smit. *Understanding Molecular Simulation*. Academic Press, London, second edition, 2002.

[7] R. Car and M. Parrinello. Unified Approach for Molecular Dynamics and Density-Functional Theory. *Phys. Rev. Lett.*, 55(22):2471–2474, 1985.

[8] M. Ceriotti. *A novel framework for enhanced molecular dynamics based on the generalized Langevin equation*. PhD thesis, ETH Zürich, 2010.

[9] M. Ceriotti, G. Bussi, and M. Parrinello. Colored-Noise Thermostats à la Carte. *J. Chem. Theory Comput.*, 6(4):1170–1180, 2010.

[10] M. Ceriotti, G. Bussi, and M. Parrinello. Langevin Equation with Colored Noise for Constant-Temperature Molecular Dynamics Simulations. *Phys. Rev. Lett.*, 102(2):020601, 2009.

[11] M. Ceriotti, M. Parrinello, T. E. Markland, and D. E. Manolopoulos. Efficient stochastic thermostatting of path integral molecular dynamics. *J. Chem. Phys.*, 133(12):124104, 2010.

[12] J. A. Morrone, T. E. Markland, M. Ceriotti, and B. J. Berne. Efficient multiple time scale molecular dynamics: Using colored noise thermostats to stabilize resonances. *J. Chem. Phys.*, 134(1):14103, 2011.

[13] M. Ceriotti, G. Bussi, and M. Parrinello. Nuclear Quantum Effects in Solids Using a Colored-Noise Thermostat. *Phys. Rev. Lett.*, 103(3):30603, 2009.

[14] M. Ceriotti, D. E. Manolopoulos, and M. Parrinello. Accelerating the convergence of path integral dynamics with a generalized Langevin equation. *J. Chem. Phys.*, 134(8):84104, 2011.

[15] M. Ceriotti and D. E. Manolopoulos. Efficient First-Principles Calculation of the Quantum Kinetic Energy and Momentum Distribution of Nuclei. *Phys. Rev. Lett.*, 109(10):100604, 2012.

[16] G. Harp and B. Berne. Time-Correlation Functions, Memory Functions, and Molecular Dynamics. *Phys. Rev. A*, 2(3):975–996, 1970.

[17] H. C. Andersen. Molecular dynamics simulations at constant pressure and/or temperature. *J. Chem. Phys.*, 72(4):2384–2393, 1980.

[18] H. J. C. Berendsen, J. P. M. Postma, W. F. Van Gunsteren, A. DiNola, and J. R. Haak. Molecular dynamics with coupling to an external bath. *J. Chem. Phys.*, 81(8):3684, 1984.

[19] S. Nose. A unified formulation of the constant temperature molecular dynamics methods. *J. Chem. Phys.*, 81(1):511, 1984.

[20] W. Hoover. Constant-pressure equations of motion. *Phys. Rev. A*, 34(3):2499–2500, 1986.

[21] G. J. Martyna, M. E. Tuckerman, and M. L. Klein. Nos{é}-Hoover chains: The canonical ensemble via continuous dynamics. *J. Chem. Phys.*, 97(4):2635, 1992.

[22] T. Schneider and E. Stoll. Molecular-dynamics study of a three-dimensional one-component model for distortive phase transitions. *Phys. Rev. B*, 17(3):1302–1322, 1978.

[23] T. Soddemann, B. Dünweg, and K. Kremer. Dissipative particle dynamics: A useful thermostat for equilibrium and nonequilibrium molecular dynamics simulations. *Phys. Rev. E*, 68(4):46702, 2003.

[24] G. Bussi, D. Donadio, and M. Parrinello. Canonical sampling through velocity rescaling. *J. Chem. Phys.*, 126(1):14101, 2007.

[25] P. Langevin. The theory of Brownian movement. *CR Acad. Sci*, 146:530, 1908.

[26] C. W. Gardiner. *Handbook of Stochastic Methods*. Springer, Berlin, third edition, 2003.

[27] R. Kubo. The fluctuation-dissipation theorem. *Reports Prog. Phys.*, 29(1):255–284, 1966.

[28] B. J. Berne and D. Forster. Topics in Time-Dependent Statistical Mechanics. *Annu. Rev. Phys. Chem.*, 22(1):563–596, 1971.

[29] R. J. Henery. The generalized Langevin equation. *J. Phys. A Gen. Phys.*, 5(9):1312–1319, 1972.

[30] R. F. Fox. Stochastic calculus in physics. *J. Stat. Phys.*, 46(5-6):1145–1157, 1987.

[31] R. Zwanzig. *Nonequilibrium statistical mechanics*. Oxford University Press, New York, 2001.

[32] J. Luczka. Non-Markovian stochastic processes: Colored noise. *Chaos*, 15(2):26107, 2005.

[33] L. Kantorovich. Generalized Langevin equation for solids. I. Rigorous derivation and main properties. *Phys. Rev. B*, 78(9):94304, 2008.

[34] M. Ottobre, G. Pavliotis, and K. Pravda-Starov. Exponential return to equilibrium for hypoelliptic quadratic systems. *J. Funct. Anal.*, 262(9):4000–4039, 2012.

[35] F. Marchesoni and P. Grigolini. On the extension of the Kramers theory of chemical relaxation to the case of nonwhite noise. *J. Chem. Phys.*, 78(10):6287, 1983.

[36] L. Stella, C. Lorenz, and L. Kantorovich. The generalized langevin equation: an efficient approach to non-equilibrium molecular dynamics of open systems. *arXiv preprint arXiv:1312.4903*, 2013.

[37] A. D. Baczewski and S. D. Bond. Numerical integration of the extended variable generalized langevin equation with a positive prony representable memory kernel. *The Journal of Chemical Physics*, 139(4):044107, 2013.

[38] J. A. Nelder and R. Mead. A Simplex Method for Function Minimization. *Comput. J.*, 7 (4):308–313, 1965.

[39] S. Habershon, T. E. Markland, and D. E. Manolopoulos. Competing quantum effects in the dynamics of a flexible water model. *J. Chem. Phys.*, 131(2):24501, 2009.

[40] M. Sprik. Computer simulation of the dynamics of induced polarization fluctuations in water. *J. Phys. Chem.*, 95(6):2283–2291, 1991.

[41] S. W. Rick, S. J. Stuart, and B. J. Berne. Dynamical fluctuating charge force fields: Application to liquid water. *J. Chem. Phys.*, 101(7):6141–6156, 1994.

[42] L. Rosso, P. Mináry, Z. Zhu, and M. E. Tuckerman. On the use of the adiabatic molecular dynamics technique in the calculation of free energy profiles. *J. Chem. Phys.*, 116(11):4389, 2002.

[43] J. VandeVondele and U. Rothlisberger. Canonical Adiabatic Free Energy Sampling (CAFES): A Novel Method for the Exploration of Free Energy Surfaces . *J. Phys. Chem. B*, 106:203–208, 2002.

[44] L. Maragliano and E. Vanden-Eijnden. A temperature accelerated method for sampling free energy and determining reaction pathways in rare events simulations. *Chem. Phys. Lett.*, 426(1-3):168–175, 2006.

[45] W. Streett, D. Tildesley, and G. Saville. Multiple time-step methods in molecular dynamics. *Mol. Phys.*, 35(3):639–648, 1978.

[46] M. Tuckerman, B. J. Berne, and G. J. Martyna. Reversible multiple time scale molecular dynamics. *J. Chem. Phys.*, 97(3):1990, 1992.

[47] R. P. Steele. Multiple-timestep ab initio molecular dynamics with electron correlation. *J. Chem. Phys.*, 139(1):011102, 2013.

[48] N. Luehr, T. E. Markland, and T. J. Martinez. Multiple time step integrators in ab initio molecular dynamics. *arXiv preprint arXiv:1312.1284*, 2013.

[49] T. Schlick, M. Mandziuk, R. D. Skeel, and K. Srinivas. Nonlinear Resonance Artifacts in Molecular Dynamics Simulations. *J. Comput. Phys.*, 140(1):1–29, 1998.

[50] E. Barth and T. Schlick. Overcoming stability limitations in biomolecular dynamics. I. Combining force splitting via extrapolation with Langevin dynamics in LN. *J. Chem. Phys.*, 109(5):1617, 1998.

[51] J. A. Izaguirre, S. Reich, and R. D. Skeel. Longer time steps for molecular dynamics. *J. Chem. Phys.*, 110(20):9853, 1999.

[52] M. Ceriotti and M. Parrinello. The δ-thermostat: selective normal-modes excitation by colored-noise Langevin dynamics. *Procedia Comput. Sci.*, 1(1):1607–1614, 2010.

[53] M. Nava, M. Ceriotti, C. Dryzun, and M. Parrinello. Evaluating functions of positive-definite matrices using colored-noise thermostats. *Phys. Rev. E*, 89(2):023302, 2014.

[54] S. Habershon and D. E. Manolopoulos. Zero point energy leakage in condensed phase dynamics: An assessment of quantum simulation methods for liquid water. *J. Chem. Phys.*, 131(24):244518, 2009.

[55] H. Dammak, Y. Chalopin, M. Laroche, M. Hayoun, and J.-J. Greffet. Quantum Thermal Bath for Molecular Dynamics Simulation. *Phys. Rev. Lett.*, 103(19):190601, 2009.

[56] N. Bedoya, J.-L. Barrat, and D. Rodney. Computation of the thermal conductivity using classical and quantum molecular dynamics based methods. *arXiv preprint arXiv:1307.2409*, 2013.

[57] R. P. Feynman and A. R. Hibbs. *Quantum Mechanics and Path Integrals*. McGraw-Hill, New York, 1964.

[58] S. A. Egorov, E. Gallicchio, and B. J. Berne. The simulation of electronic absorption spectrum of a chromophore coupled to a condensed phase environment: Maximum entropy versus singular value decomposition approaches. *J. Chem. Phys.*, 107(22):9312, 1997.

[59] S. Habershon, B. J. Braams, and D. E. Manolopoulos. Quantum mechanical correlation functions, maximum entropy analytic continuation, and ring polymer molecular dynamics. *J. Chem. Phys.*, 127(17):174108, 2007.

[60] T. M. Yamamoto. Path-integral virial estimator based on the scaling of fluctuation coordinates: Application to quantum clusters with fourth-order propagators. *J. Chem. Phys.*, 123(10):104101, 2005.

[61] L. Lin, J. A. Morrone, R. Car, and M. Parrinello. Displaced Path Integral Formulation for the Momentum Distribution of Quantum Particles. *Phys. Rev. Lett.*, 105(11):110602, 2010.

[62] M. Ceriotti and T. E. Markland. Efficient methods and practical guidelines for simulating isotope effects. *J. Chem. Phys.*, 138(1):014112, 2013.

[63] M. Suzuki. Hybrid exponential product formulas for unbounded operators with possible applications to Monte Carlo simulations. *Phys. Lett. A*, 201(5-6):425–428, 1995.

[64] S. A. Chin. Symplectic integrators from composite operator factorizations. *Phys. Lett. A*, 226(6):344–348, 1997.

[65] A. Pérez and M. E. Tuckerman. Improving the convergence of closed and open path integral molecular dynamics via higher order Trotter factorization schemes. *J. Chem. Phys.*, 135 (6):064104, 2011.

[66] M. Ceriotti, G. a. R. Brain, O. Riordan, and D. E. Manolopoulos. The inefficiency of reweighted sampling and the curse of system size in high-order path integration. *Proc. R. Soc. A Math. Phys. Eng. Sci.*, 468(2137):2–17, 2011.

[67] M. E. Tuckerman, D. Marx, M. L. Klein, and M. Parrinello. Efficient and general algorithms for path integral Car-Parrinello molecular dynamics. *J. Chem. Phys.*, 104(14):5579–5588, 1996.

[68] S. Jang and G. A. Voth. Simple reversible molecular dynamics algorithms for Nosé-Hoover chain dynamics. *J. Chem. Phys.*, 107(22):9514–9526, 1997.

[69] G. Bussi and M. Parrinello. Accurate sampling using Langevin dynamics. *Phys. Rev. E*, 75(5):56707, 2007.

[70] R. F. Fox, I. R. Gatland, R. Roy, and G. Vemuri. Fast, accurate algorithm for numerical simulation of exponentially correlated colored noise. *Phys. Rev. A*, 38(11):5938–5940, 1988.

[71] T. D. Kühne, M. Krack, F. R. Mohamed, and M. Parrinello. Efficient and Accurate Car-Parrinello-like Approach to Born-Oppenheimer Molecular Dynamics. *Phys. Rev. Lett.*, 98 (6):066401, 2007.

[72] M. Ceriotti. GLE4MD. http://gle4md.berlios.de, 2010.

[73] A. Witt, S. D. Ivanov, M. Shiga, H. Forbert, and D. Marx. On the applicability of centroid and ring polymer path integral molecular dynamics for vibrational spectroscopy. *J. Chem. Phys.*, 130(19):194510, 2009.

[74] M. Ceriotti, J. More, and D. E. Manolopoulos. i-PI: A Python interface for ab initio path integral molecular dynamics simulations. *Comput. Phys. Commun.*, 185:1019–1026, 2014.

[75] CPMD. http://www.cpmd.org/.

[76] CP2K. http://www.cp2k.org.

[77] P. Giannozzi, S. Baroni, N. Bonini, M. Calandra, R. Car, C. Cavazzoni, D. Ceresoli, G. L. Chiarotti, M. Cococcioni, I. Dabo, A. D. Corso, S. de Gironcoli, S. Fabris, G. Fratesi, R. Gebauer, U. Gerstmann, C. Gougoussis, A. Kokalj, M. Lazzeri, L. Martin-Samos, N. Marzari, F. Mauri, R. Mazzarello, S. Paolini, A. Pasquarello, L. Paulatto, C. Sbraccia, S. Scandolo, G. Sclauzero, A. P. Seitsonen, A. Smogunov, P. Umari, and R. M. Wentzcovitch. QUANTUM ESPRESSO: a modular and open-source software project for quantum simulations of materials. *J. Phys. Condens. Matter*, 21(39):395502–395519, 2009.

[78] V. Blum, R. Gehrke, F. Hanke, P. Havu, V. Havu, X. Ren, K. Reuter, and M. Scheffler. Ab initio molecular simulations with numeric atom-centered orbitals. *Comput. Phys. Commun.*, 180(11):2175–2196, 2009.

[79] J. F. Herbst and L. G. Hector Jr. Energetics of the Li amide/Li imide hydrogen storage reaction. *Phys. Rev. B*, 72(12):125120, 2005.

[80] G. Miceli, M. Ceriotti, M. Bernasconi, and M. Parrinello. Static disorder and structural correlations in the low-temperature phase of lithium imide. *Phys. Rev. B*, 83(5):54119, 2011.

[81] T. Mueller and G. Ceder. Ab initio study of the low-temperature phases of lithium imide. *Phys. Rev. B*, 82(17):174307, 2010.

[82] M. Ceriotti, G. Miceli, A. Pietropaolo, D. Colognesi, A. Nale, M. Catti, M. Bernasconi, and M. Parrinello. Nuclear quantum effects in ab initio dynamics: Theory and experiments for lithium imide. *Phys. Rev. B*, 82(17):174306, 2010.

[83] C. Andreani, D. Colognesi, J. Mayers, G. F. Reiter, and R. Senesi. Measurement of momentum distribution of light atoms and molecules in condensed matter systems using inelastic neutron scattering. *Adv. Phys.*, 54(5):377–469, 2005.

[84] G. F. Reiter, R. Senesi, and J. Mayers. Changes in the Zero-Point Energy of the Protons as the Source of the Binding Energy of Water to A-Phase DNA. *Phys. Rev. Lett.*, 105(14): 148101, 2010.

[85] M. Krzystyniak and F. Fernandez-Alonso. Ab initio nuclear momentum distributions in lithium hydride: Assessing nonadiabatic effects. *Phys. Rev. B*, 83(13):134305, 2011.

[86] A. G. Seel, M. Ceriotti, P. P. Edwards, and J. Mayers. Simultaneous measurement of lithium and fluorine momentum in 7LiF. *J. Phys. Condens. Matter*, 24(36):365401, 2012.

[87] A. A. Hassanali, J. J. Cuny, M. Ceriotti, C. J. Pickard, and M. Parrinello. The Fuzzy Quantum Proton in the Hydrogen Chloride Hydrates. *J. Am. Chem. Soc.*, 134(20):8557–8569, 2012.

[88] A. Hassanali, M. K. Prakash, H. Eshet, and M. Parrinello. On the recombination of hydronium and hydroxide ions in water. *Proc. Natl. Acad. Sci. USA U. S. A.*, 108(51):20410–5, 2011.

[89] R. Z. Khaliullin, H. Eshet, T. D. Kühne, J. Behler, and M. Parrinello. Graphite-diamond phase coexistence study employing a neural-network mapping of the ab initio potential energy surface. *Phys. Rev. B*, 81(10):100103, 2010.

[90] R. Ramírez and C. P. Herrero. Quantum path integral simulation of isotope effects in the melting temperature of ice Ih. *J. Chem. Phys.*, 133(14):144511, 2010.

[91] D. Colognesi. Extraction of single-particle mean kinetic energy from macroscopic thermodynamic data. *Phys. B Condens. Matter*, 406(14):2723–2730, 2011.

[92] X.-Z. Li, B. Walker, and A. Michaelides. Quantum nature of the hydrogen bond. *Proc. Natl. Acad. Sci. USA*, 108(16):6369–6373, 2011.

[93] T. E. Markland and B. J. Berne. Unraveling quantum mechanical effects in water using isotopic fractionation. *Proc. Natl. Acad. Sci. USA*, 109(21):7988–7991, 2012.

[94] G. Romanelli, M. Ceriotti, D. E. Manolopoulos, C. Pantalei, R. Senesi, and C. Andreani. Direct Measurement of Competing Quantum Effects on the Kinetic Energy of Heavy Water upon Melting. *J. Phys. Chem. Lett.*, 4(19):3251–3256, 2013.

[95] M. Ceriotti, J. Cuny, M. Parrinello, and D. E. Manolopoulos. Nuclear quantum effects and hydrogen bond fluctuations in water. *Proc. Natl. Acad. Sci. USA U. S. A.*, 110(39): 15591–6, 2013.

[96] S. Fritsch, R. Potestio, D. Donadio, and K. Kremer. Nuclear quantum effects in water: A multi-scale study. *J. Chem. Theory Comput.*, 2014.